Journal of Advanced Research 83 (2026) 1061–1081

Contents lists available at ScienceDirect

Journal of Advanced Research

journal homepage: www.elsevier.com/locate/jare

Enhanced tuberculosis control via leveraging dendritic cell-mediated Th1 responses in preventive and immunotherapeutic vaccine strategies

Hongmin Kim [a,1], Jong-Seok Kim [a,b,1], Kee Woong Kwon [a,c], Woo Sik Kim [a,d], Minchul Park [e,f], Sang-Jun Ha [e,f], Sangwon Choi [a,g], Jiseon Kim [h], Sung Jae Shin [a,g,*]

[a] Department of Microbiology, Institute for Immunology and Immunological Disease, Yonsei University College of Medicine, Seoul, South Korea
[b] Myunggok Medical Research Institute, College of Medicine, Konyang University, Daejeon, South Korea
[c] Department of Microbiology, College of Medicine, Gyeongsang National University, Jinju, South Korea
[d] Functional Biomaterial Research Center, Korea Research Institute of Bioscience and Biotechnology, Jeongeup-si, Jeollabuk-do, South Korea
[e] Department of Biochemistry, College of Life Science and Biotechnology, Yonsei University, Seoul, South Korea
[f] Brain Korea 21(BK21) Four program, Yonsei Education & Research Center for Biosystems, Yonsei University, Seoul, South Korea
[g] Graduate School of Medical Science, Brain Korea 21 Project, Yonsei University College of Medicine, Seoul, South Korea
[h] Department of Biomedical Sciences, Graduate School of Medical Science, Brain Korea 21 Project, Yonsei University College of Medicine, Seoul, South Korea

HIGHLIGHTS

- Adoptive transfer of DCs stimulated with CFA of Mtb enhances BCG vaccine efficacy within one week post-Mtb infection.
- CFA-DC transfer following BCG vaccination enhances multifunctional CD4$^+$ T cell responses in the lung parenchyma.
- CFA-DC transfer provides prolonged vaccine efficacy for BCG against Mtb infection.
- CFA-DC transfer enhances the antibiotic efficacy by supporting CD4$^+$ T cell responses and improving treatment outcomes.
- CFA-DC transfer protects against Mtb reactivation, including multidrug-resistant Mtb strains.

GRAPHICAL ABSTRACT

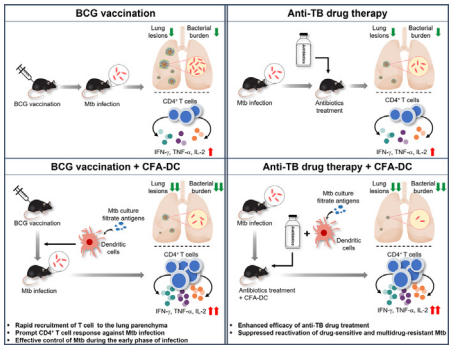

ARTICLE INFO

Article history:
Received 11 January 2025
Revised 3 July 2025
Accepted 28 July 2025
Available online 30 July 2025

Keywords:
Tuberculosis
BCG
Booster vaccine
DC-based immunotherapy

ABSTRACT

Introduction: Insufficient vaccine efficacy of the Bacillus Calmette-Guérin (BCG) and long, expensive tuberculosis (TB) treatments highlight the need for better TB control measures.
Methods: This study evaluated whether the adoptive transfer of dendritic cell (DC)-based vaccines pulsed with culture filtrate antigens (CFA) of *Mycobacterium tuberculosis* (Mtb) could enhance BCG efficacy and support anti-TB drug therapy.
Results: In BCG-vaccinated mice, adoptive transfer of CFA-pulsed DCs promoted swift T cell recruitment to the lung parenchyma, reducing bacterial load within 1 week post-infection, promoting the generation of tissue-resident T cells and expansion of CD4$^+$ T cells co-producing IFN-γ, IL-2, and/or TNF-α. The vaccine efficacy persisted for a prolonged period post-infection, with protection found in both high dose and low dose Mtb infection models. Additionally, CFA-DC administration during chemotherapy enhanced

* Corresponding author at: Department of Microbiology, Institute for Immunology and Immunological Disease, Graduate School of Medical Science, Brain Korea 21 Project, Yonsei University College of Medicine, Seoul, South Korea.
E-mail address: sjshin@yuhs.ac (S.J. Shin).
[1] These authors contributed equally to the work.

https://doi.org/10.1016/j.jare.2025.07.056
2090-1232/

Multifunctional T cell
Reactivation

treatment efficacy, maintaining CD4$^+$ T cell responses. In latent TB models, mice were protected from Mtb reactivation in both drug-sensitive and multidrug-resistant TB models.
Conclusions: DC-based prophylactic and immunotherapeutic vaccine strategies enhance protective immunity during BCG vaccination and chemotherapy, offering new insights into TB control strategies.

Introduction

Tuberculosis (TB), driven by the pathogen *Mycobacterium tuberculosis* (Mtb), remains a significant global health challenge in the 21st century, characterized by its enduring prevalence and substantial impacts on morbidity and mortality. This highly successful human-adapted pathogen caused approximately 10.8 million new cases and approximately 1.25 million deaths in 2023 [1]. The Bacillus Calmette-Guérin (BCG), currently the sole licensed vaccine for TB, is broadly administered but provides limited protection that diminishes over time, typically lasting only until adolescence [2]. Treating TB requires prolonged antibiotic regimens, and the rise of antibiotic-resistant Mtb strains further complicates disease control [3]. Furthermore, since the COVID-19 pandemic, the global incidence of new TB cases and related deaths has risen [1]. The COVID-19 pandemic has disrupted TB care and prevention around the world including sharp drop in diagnosis and case notifications, delays in treatment initiation, and decrease in BCG coverage among children [4]. Emerging evidence suggests that SARS-CoV-2 infection may accelerate TB progression by depleting CD4$^+$ T cells and promoting detrimental lung inflammation [5]. This situation underscores the urgent need for novel vaccines and advanced therapeutic approaches to enhance TB management.

T cell immunity, particularly involving CD4$^+$ T cells, plays a pivotal role in controlling TB. A distinctive characteristic of TB, the delayed accumulation of lung CD4$^+$ T cells, is observed following Mtb infection [6]. Mtb-mediated inhibition of antigen (Ag) presentation by Ag-presenting cells (APCs) is thought to play a role in causing the delayed T cell response [7]. To direct swift T cell responses, lung dendritic cells (DCs) are required to migrate to lymph nodes (LNs) and subsequently present Ags to naïve T cells [7]. Consequently, it is crucial for DCs to rapidly detect Mtb infection and facilitate timely immune responses through their swift migration to LNs. However, reports on the functions of DC subsets in mouse models of TB remain controversial [8,9], indicating the need for further investigation into DC subsets to advance TB control, particularly in the development of effective vaccines and immunotherapeutics.

Adjunctive therapies aim to reduce treatment duration, enhance therapeutic outcomes, and ultimately prevent relapse. Immunotherapeutic vaccination, developed to augment the host T cell response, has been utilized as an adjuvant to antibiotic regimens, improving Mtb control in both patients and animal models [10,11]. Furthermore, the administration of key Th1-related cytokines, such as IFN-γ and IL-12 have been shown to improve the control of bacterial growth and reduce tissue injury in TB patients [12]. These results indicate that the host immune response is pivotal in influencing anti-TB treatment outcome. However, reports that antibiotics used in anti-TB therapy, such as isoniazid (INH) or clofazimine (CFZ), curtail the immune responses imply that immunological intervention is necessary for efficient treatment [13,14].

TB presents a broad disease spectrum, ranging from presumed latent TB infection to early-stage TB, subclinical TB, active cavitary disease, and post-TB lung disease [15]. Furthermore, the Mtb genotype influences multiple aspects of TB progression [16], such as multidrug resistance (MDR) development and treatment outcomes, with the Beijing genotype notably associated with reduced BCG vaccine efficacy, higher relapse rates, and an increased propensity for MDR development [17,18]. Therefore, developing TB control strategies applicable across the entire TB spectrum would be highly valuable. Although animal model studies have predominantly focused on DCs during the early period of infection, DCs persist throughout the infection and continue to exert influence across all stages [19,20]. Following the establishment of the acquired immunity and the formation of granulomas, DCs continuously acquire Mtb-Ag and are replaced during Ag sampling to guide T cell responses as they migrate in and out of the granulomas [19]. Furthermore, they contribute to the generation of new granulomas by forming clusters with T cells outside granulomas across both the acute and chronic phases of BCG or Mtb infections [20]. Additionally, the Mtb-Ag repertoire varies across infection stages [21], underscoring the pivotal role of DCs in shaping T cell immunity throughout the TB spectrum.

Finely tuned DC-targeting TB control strategies that can modulate core T cell immunity across a diverse spectrum have potential applications in vaccines and immunotherapy. For example, DC-targeted Ag85B vaccination or DC transfer in BCG-primed mice accelerated T cell activation and improved control of Mtb [22,23]. Moreover, combining therapeutic vaccination with antibiotics extended Th1 responses and enhanced treatment efficacy [24], suggesting that DC-targeted strategies as promising approaches for TB prophylaxis, treatment enhancement, and relapse prevention.

In this study, we propose effective TB control strategies that utilize the adoptive transfer of Mtb-Ag-loaded DCs in conjunction with BCG vaccination and antibiotic treatment to address the broad TB spectrum. The transfer of Mtb-Ag-loaded DCs was shown to improve the BCG vaccine efficacy, as evidenced across various clinical strains. This approach also enhanced Ag-specific multifunctional CD4$^+$ T cells in the lung by directing their localization to the parenchymal region during the early phase of Mtb infection and resulted in durable protection. Additionally, DC transfer during antibiotic therapy not only improved the efficacy of antibiotics by amplifying Ag-specific CD4$^+$ T cell responses but also inhibited Mtb growth in lung tissue in a relapse model following antibiotic treatment. Furthermore, this strategy demonstrated effectiveness against MDR-TB. Collectively, this study expands DC-based TB strategies by incorporating therapeutic applications, including diverse clinical strains, dose-dependent infection models, varied intervals between vaccination and boosting, antibiotic combinations, and relapse control. The findings highlight the critical role of DCs in TB prevention and treatment and offer valuable insights for future TB control strategies.

Material and Methods

Study approval

Animal experiments were conducted in accordance with the established guidelines of the Korea Centers for Disease Control and Prevention (KCDC) and the Korean Food and Drug Administration (KFDA). The experimental procedures in this study received approval from the Ethics Committee and the Institutional Animal Care and Use Committee (Permit Numbers: 2021–0279, 2019–0046, 2015–0273) of the Laboratory Animal Research Center at Yonsei University College of Medicine (Seoul, Korea).

Animals

Specific pathogen-free mice (C57BL6/J, female), aged 6 to 7 weeks, were obtained from Japan SLC, Inc. (Shizuoka, Japan). The mice were housed in the Animal Biosafety Level 3 at the Avison Biomedical Research Center, Yonsei University College of Medicine. The mice were housed in a controlled environment with a maintained at 24 ± 1°C and 50 ± 5 % humidity, following a 12-h light–dark cycle (lights activated at 7 am and deactivated at 7 pm). The mice were supplied with a sterile commercial feed and had unlimited access to water.

Reagents

Mouse recombinant granulocyte–macrophage colony-stimulating factor (GM-CSF) and IL-4 were obtained from Creagene (Seoul, Korea). Fms-like tyrosine kinase 3 (FLT3) ligand, expressed in a Chinese hamster ovary cell line, was generously provided by Professor Park CG at Yonsei University. Purified protein derivative (PPD) was generously provided by Dr. Brennan at Aeras (Rockville, MD, USA). Rifampicin (RIF), INH, and CFZ were obtained from Sigma-Aldrich (St. Louis, MO, USA). Pam3CSK4 was obtained from InvivoGen (San Diego, California, USA). Anti-MHC Class II microbeads and anti-CD11b microbeads were purchased from Miltenyi Biotec (Bergisch Gladbach, Germany). The culture filtrate Ags (CFA) from individual Mtb strains were prepared as described previously [25].

Preparation of mycobacteria strains

The HN878 strain of Mtb was sourced from BEI Resources of ATCC (Manassas, VA, USA). Mtb K strain was sourced from the Korean Institute of Tuberculosis (KIT, Osong, Chungcheongbuk-do, Korea). The Erdman strain of Mtb and INH and RIF resistant MDR-Mtb (A008) were sourced from the International Tuberculosis Research Center (ITRC, Changwon, Gyeongsangnam-do, Korea). *M. bovis* BCG (Pasteur 1173P2) was generously provided by Dr. Brosch at the Pasteur Institute (Paris, France). The Mtb H37Rv (ATCC 27294) strain was sourced from ATCC (Manassas, VA, USA). The cultivation of mycobacterial strains was performed following previously established protocols [26].

Preparation of bone marrow-derived DC subsets

Bone marrow cells were isolated from the femur and tibia of specific pathogen-free mice (C57BL6/J, female) and bone marrow-derived DCs (BMDCs) were differentiated with GM-CSF/IL-4 (GM-DC) as previously described [27]. For DCs differentiated with FLT3 ligand, bone marrow cells were re-suspended at 4×10^6 cells in FLT3 ligand containing media (300 ng/ml). Fresh medium containing FLT3 ligand (300 ng/ml) was added at 5 days, and cells were harvested on day 8 and sorted into $CD11b^+$ (FL-DC1) and $CD11b^-$ DC (FL-DC2) subpopulations for experiments. To prepare DCs for *in vitro* experiments and in adoptive transfer, the cells were stimulated with Mtb-CFA (50 μg/ml) for 24 h. For certain experiment, DCs were stimulated with Pam3 (100 ng/ml). DCs were washed with PBS, and each mouse received 1×10^6 DCs in 200 μl via intravenous (IV) injection.

BCG immunization, Mtb challenge, and adoptive transfer of DCs

To evaluate the efficacy of CFA-matured BMDCs, several Mtb strains were used for *in vivo* experiments. For 60 min, mice were exposed to a predetermined inoculum of several Mtb strains in the inhalation chamber of an airborne infection system (Glas-Col, Terre Haute, IN, USA) [28]. For BCG vaccination, 1×10^6 colony forming units (CFUs)/mouse were immunized in the subcutaneous route. After 6 or 10 weeks, 1×10^6 of DCs/mouse were adoptively transferred via IV route. After 3 days, approximately 200 CFUs of Mtb strains, unless otherwise indicated, were challenged per mouse. Approximately 1×10^5 CFUs/mouse and 10 CFUs/mouse of Mtb K were challenged for high dose and low dose Mtb challenges respectively.

Treatment regimens, adjunctive immunotherapeutic vaccination of DCs, and reactivation TB model

For the adjunctive immunotherapeutic vaccination and reactivation TB model, approximately 200 CFUs of Mtb K were challenged. In the case of MDR-Mtb, we aimed to challenge a higher dose of infection (approximately 400–––500 CFUs per mouse), since antibiotic-resistant Mtb tends to display lower virulence [29]. In the adjunctive therapeutic vaccine model, 4 weeks post-infection, BMDC differentiated with GM-CSF were administered via IV route to mice on four occasions over a 4-week antibiotic regimen, where RIF (10 mg/kg) and INH (25 mg/kg) were continuously supplied in the drinking water, refreshed every other day. After 12 weeks, the mice were sacrificed for analysis. In reactivation TB model, mice were exposed to Mtb K, and the INH and RIF were administered from 4 to 12 weeks post-infection. GM-DC was administered via IV route to mice once a week for 4 weeks starting from the 11 weeks post-infection. Reactivation was monitored after the termination of drug treatment and found to occur naturally without any pharmacological immunosuppression. The bacterial growth was measured at 23 and 35 weeks post-infection. In the MDR-Mtb infection model, mice were infected with MDR-Mtb (A008) via aerosol route and administered GM-DC weekly for 4 weeks, starting at 11 weeks post-infection. INH and RIF were continuously supplied in the drinking water, while CFZ (20 mg/kg) was administered daily through oral gavage between 4 and 14 weeks post-infection.

Intravascular staining

For intravascular staining to distinguish between vascular and tissue cells, 4 μg of a fluorescein isothiocyanate (FITC) conjugated-anti-CD45.2 monoclonal antibody (BD Biosciences, San Jose, CA, USA) was injected via IV route to the mice. The mice were euthanized 3 min later for the analysis.

Flow cytometry analysis

For every staining set, cells were initially incubated with anti-CD16/32 antibody for 20 min at 4 °C. For staining surface molecule of DC subsets, cells were stained with fluorochrome-conjugated antibodies against MHC class I (phycoerythrin, PE), CD11c (PE–Cyanine7, PE-Cy7), CD11b (Peridinin–Chlorophyll Protein–Cyanine5.5, PerCP-Cy5.5), CD86 (allophycocyanin, APC), CD80 (APC), MHC class II (PE) (Thermo Fisher Scientific, Waltham, MA, USA), CD103 (Alexa Fluor 488), and CD40 (FITC) (Biolegend, San Diego, CA, USA). To prepare single-cell suspensions, spleens and lung tissues were minced and treated at 37 °C for 30 min in RPMI 1640 digestion medium supplemented with 10 % fetal bovine serum and 0.1 % collagenase type II (Worthington, Lakewood, NJ, USA), $MgCl_2$ (1 mM), and $CaCl_2$ (1 mM). Following incubation, the cell suspensions were strained using a 40-μm nylon mesh. The cells were incubated with RBC lysis buffer (Sigma-Aldrich, St. Louis, MO, USA) for 3 min and washed twice. The cells were stained with LIVE/DEAD™ Fixable Far Red Dead Cell Stain Kit (Thermo Fisher Scientific, Waltham, MA, USA) to exclude dead cells, and stained with antibodies against Thy1.2 (Brilliant Violet 605, BV605) (BD bioscience, San Jose, CA, USA), MHC-II (Brilliant Violet 421,

BV421), CD11b (PerCP-Cy5.5), CD11c (PE/Dazzle 594), Siglec-F (Alexa Fluor 700), Ly-6G (APC-Cy7) (Biolegend, San Diego, CA, USA), and F4/80 (PE-Cy7) (Thermo Fisher Scientific, Waltham, MA, USA) for immune cell population analysis. For staining surface molecules of T cells, the cells were stained with eBioscience™ Fixable Viability Dye eFluor™ 780 (Thermo Fisher Scientific, Waltham, MA, USA) to gate out dead cells, and the cells were stained with antibodies against to CD4 (PerCP-Cy5.5), CD8a (Brilliant Violet 785, BV785), CCR6 (PE), CD69 (PE/Dazzle 594), CD44 (PE-Cy7), CXCR3 (APC), KLRG1 (BV605) (Biolegend, San Diego, CA, USA). For the memory T cells analysis, the cells were stained with eBioscience™ Fixable Viability Dye eFluor™ 780 (Thermo Fisher Scientific, Waltham, MA, USA), and the cells were stained with antibodies against CD4 (PerCP-Cy5.5), CD8a (BV785), CD44 (BV421), CD62L (Alexa Fluor 700), CD69 (PE/Dazzle 594), CD127 (PE-Cy7) (Biolegend, San Diego, CA, USA) and CD103 (APC) (Thermo Fisher Scientific, Waltham, MA, USA). After 30 min, the cells were washed with PBS, then fixed and permeabilized for 30 min at 4 °C with the transcription factor staining kit (Thermo Fisher Scientific, Waltham, MA, USA). The cells were washed, then intracellularly stained with antibody against Ki67 (PE) (Thermo Fisher Scientific, Waltham, MA, USA). After being washed with PBS, the cells were fixed and permeabilized with the transcription factor staining kit (Thermo Fisher Scientific, Waltham, MA, USA) for 30 min at 4 °C. To stain intracellular cytokines, cells were incubated for 12 h at 37 °C with PPD (2 μg/ml) in the presence of GolgiPlug and GolgiStop (Thermo Fisher Scientific, Waltham, MA, USA). Dead cells were stained with eBioscience™ Fixable Viability Dye eFluor™ 780 (Thermo Fisher Scientific, Waltham, MA, USA), and the cells were stained with antibodies against Thy1.2 (BV605) (BD Biosciences, San Jose, CA, USA), CD8a (BV785), CD4 (PerCP-Cy5.5), and CD44 (BV421) (Biolegend, San Diego, CA, USA). After 30 min, the cells were washed with PBS, then fixed and permeabilized for 30 min at 4 °C with Cytofix/Cytoperm (BD Biosciences, San Jose, CA, USA). The cells were washed, then intracellularly stained with antibodies against TNF-α (APC), IL-2 (PE-Cy7) (Thermo Fisher Scientific, Waltham, MA, USA), and IFN-γ (PE) (BD Biosciences, San Jose, CA, USA) for 30 min at 4 °C. The cells were washed and suspended in PBS for analysis with Cytoflex (Beckman-Coulter, Pasadena, CA, USA) or LSR-Fortessa-X20 (BD Biosciences, San Jose, CA, USA). A summary table and a schematic flowchart for the flow cytometry analysis are provided in Sup. Table S1.

Bacterial counts and histopathology

Bacterial burden in the lungs and spleens was quantified by plating homogenized organ suspensions onto Middlebrook 7H10 agar (BD Biosciences, San Jose, CA, USA) supplemented with 10 % OADC enrichment medium, following previously established protocols [30]. Lung tissues were fixed overnight in 10 % neutral buffered formalin, embedded in paraffin, sliced into 4–5 μm sections, and stained with hematoxylin and eosin (H&E) for histopathological examination. The inflammation severity of lung lesion was analyzed using ImageJ software (National Institutes of Health, USA) as previously described [31]. The images were converted to grayscale, with inflamed areas highlighted in black and non-inflamed areas displayed in white. The proportion of inflamed areas was calculated with ImageJ software.

Rna-seq analysis

For RNA sequencing, lung tissues were harvested 1 week post-infection with Mtb from both the BCG and BCG/GM-DC groups. Total RNA was extracted using Trizol reagent (Invitrogen, Carlsbad, CA, USA). The mRNA was isolated using the Poly(A) RNA Selection Kit (LEXOGEN, Vienna, Austria). Libraries were prepared from total RNA using the NEBNext Ultra II Directional RNA-Seq Kit (NEW ENGLAND BioLabs, Inc., Hitchin, UK). High-throughput sequencing was conducted as paired-end 100 sequencing using NovaSeq 6000 (Illumina, Inc., St. Louis, California, USA). Data analysis and visualization were conducted using ExDEGA software (Ebiogen Inc., Seoul, Korea). The resulting sequencing data were processed to align reads to the reference genome, and differential gene expression analysis was conducted. Genes with significant expression changes (fold change > 2, adjusted p-value < 0.05) were identified as differentially expressed genes. Gene Ontology (GO) analysis was conducted to determine enriched biological processes using the DAVID tool (Database for Annotation, Visualization, and Integrated Discovery, https://david.ncifcrf.gov/). Functional interaction networks were constructed using the STRING (Search Tool for the Retrieval of Interacting Genes/Proteins) database (v11.5), based on differentially expressed genes identified by RNA-seq. Gene set enrichment analysis (GSEA) was performed using GSEA software (v4.3.2; Broad Institute, Cambridge, MA, USA) with Gene Ontology Biological Process (GOBP), and WikiPathways (WP) gene sets to identify enriched pathways between groups.

Antibody titers in serum

PPD (2 μg/ml) was used to coat the plates, and the serum sample were incubated overnight at 4 °C. Horseradish peroxidase (HRP)-conjugated anti-IgG1 (BD Biosciences) or anti-IgG2c (Southern Biotech, Birmingham, AL, USA) antibodies were used as secondary antibodies. The reaction was stopped, and the optical density was measured at 450 nm using a microplate ELISA reader.

Immunohistochemistry staining

The slides were passed through xylene; 100 %, 95 %, and 70 % ethanol; and distilled water for deparaffinization and rehydration. To perform Ag retrieval, pH 6.0 citrate buffer (DAKO S1699; Agilent Technologies, Santa Clara, CA, USA) was used at a high temperature in a high-pressure cooker and then cooled on ice for 1 h. The slides were treated with 3 % H_2O_2 in PBS for 30 min to block endogenous peroxidase activity, followed by treatment with mouse-on-mouse blocking reagent (Vector Laboratories, Burlingame, CA, USA) for 1 h, and incubated with the following mouse primary antibodies at 4 ∘C overnight: anti-neutrophil (ab2557, Abcam, Cambridge, UK), F4/80 (70076, Cell signaling, Danvers, MA, USA), CD3ε (ab5690, Abcam, Cambridge, UK), B220 (ab64100, Abcam, Cambridge, UK). The slides were treated with a protein-blocking solution (DAKO, Agilent Technologies, Santa Clara, CA, USA) for 1 h and then incubated with an HRP-conjugated secondary antibody (DAKO, Agilent Technologies, Santa Clara, CA, USA) for 15 min. A DAB substrate (DAKO, Agilent Technologies, Santa Clara, CA, USA) was used to develop the immunohistochemistry signal and the slides were dipped into Mayer's hematoxylin for nuclear staining.

Sirius Red staining

For Sirius Red staining, tissue sections were deparaffinized by immersing them three times in xylene and then rehydrated through a graded ethanol series (100 %, 95 %, and 70 %). The sections were stained with Picro Sirius Red solution (Scytek, Logan, Utah, USA) for 1 h, followed by two washes in 0.5 % acetic acid. After staining, the slides were dehydrated in ascending concentrations of ethanol (95 % and 100 %, 1 min each) and cleared in xylene for 10 min. Finally, the slides were mounted using a mounting medium (Thermo Scientific, Waltham, MA, USA) and visualized under a light microscope.

Immunofluorescence staining

Paraffin-embedded lung tissues were sectioned at a thickness of 4 μm. The sections were deparaffinized in xylene and subjected to Ag retrieval in citrate buffer (pH 6.0) at sub-boiling temperature for 20 min. After cooling and washing with PBS, the sections were blocked with 5 % normal goat serum for 1 h at room temperature. Subsequently, the sections were incubated overnight at 4 °C with the following primary antibodies: anti-PD-1 (clone RMP1-14, Leinco Technologies, Missouri, USA), FITC-conjugated anti-CD3 (clone 145-2C11, Invitrogen), and PE-conjugated anti-Tim-3 (clone 215008, R&D Systems, Minneapolis, USA). After washing, sections were incubated with Alexa Fluor™ 594-conjugated goat anti-rat IgG (H + L) secondary antibody (Invitrogen, Carlsbad, CA, USA) for 1 h at room temperature. Nuclei were counterstained with DAPI (4′,6-diamidino-2-phenylindole, 1 μg/mL), and sections were mounted using Vectashield mounting medium (Vector Laboratories, Burlingame, USA).

Stained tissues were imaged using a Leica THUNDER Imager DMi8 fluorescence microscope equipped with a 40 × objective lens. For high-resolution visualization, a Zeiss LSM 700 confocal laser scanning microscope was used. Fluorescence intensity was quantified using ImageJ software.

Statistical analysis

Statistical significance between two groups was analyzed using unpaired Student's *t*-tests, while differences among three or more groups were analyzed using one-way analysis of variance (ANOVA) with Tukey's multiple comparison test. Statistical significance in survival test was analyzed using the Log-rank (Mantel-Cox) test. GraphPad Prism version 8.00 (GraphPad Software, San Diego, CA, USA) was used for all statistical analysis. Statistical significance was determined at $^{*}p < 0.05$, $^{**}p < 0.01$, and $^{***}p < 0.001$.

Results

Adoptive transfer of DCs facilitates early TB control via CD4$^+$ T cell responses

DC subsets exhibit distinct phenotypic characteristics and functions in generating T cell responses during Mtb infection [32], thus we first differentiated BMDC subsets using FLT3 ligand (FL-DC) and GM-CSF (GM-DC) to evaluate the protective effect of adoptive transfer of DCs in BCG-vaccinated mice. FL-DC subsets could be differentiated into at least two subpopulations of DCs based on CD11b expression levels [33]. Two subsets, XCR-1$^-$CD11b$^+$ DCs (FL-DC1) and XCR-1$^+$CD11b$^-$ DCs (FL-DC2) were collected by using magnetic bead cell separation **(Supplementary Fig. 1A, B)**. FL-DC1, FL-DC2, and GM-DC were stimulated with Mtb CFA for 24 h, and cytokine secretion profiles and expression of surface molecules were analyzed **(Supplementary Fig. 1C-E)**. GM-DCs displayed enhanced secretion of cytokines, including TNF-α, IL-1β, and IL-12, and increased expression of surface molecules such as CD40, CD80, and CD103 relative to FL-DC1 and FL-DC2 **(Supplementary Fig. 1C-E)**. This indicates that GM-DCs exhibit the highest functional maturation status in response to the secreted Ag pool of Mtb.

To evaluate the efficacy of adoptive transfer of Mtb-Ag-primed DC subsets against Mtb infection in BCG-vaccinated mice, we first vaccinated mice subcutaneously with BCG, followed by the adoptive transfer of 1×10^6 cells of GM-DC, FL-DC1, or FL-DC2 stimulated with CFA into the mice 10 weeks post-BCG vaccination (Fig. 1**A**). Three days after DC administration, mice were challenged with Mtb H37Rv via the aerosol route. To screen whether each DC subset is able to boost existing protective immunity conferred by BCG vaccination, we selected 6 weeks post-infection time points commonly applied in TB vaccine efficacy assessments [34,35]. As a result, the BCG-vaccinated group exhibited a reduction in pulmonary pathological lesions relative to the unvaccinated group (Fig. 1**B**). The BCG-prime/FL-DC1-boost (BCG/FL-DC1) and BCG-prime/FL-DC2-boost (BCG/FL-DC2) groups did not exhibit enhanced protective effects against lung lesions compared to the BCG group. However, the BCG-prime/GM-DC-boost (BCG/GM-DC) group demonstrated a significant reduction in the inflammatory area (Fig. 1**B**). One week post-infection, the BCG/GM-DC group showed a reduced bacterial burden of lungs relative to the BCG, BCG/FL-DC1, and BCG/FL-DC2 groups, suggesting that GM-DC administration facilitates early recognition and response to Mtb infection. At 6 weeks post-infection, the BCG/FL-DC1, BCG/FL-DC2, and BCG/GM-DC groups showed reductions in bacterial loads in the lungs and spleen compared to the infection group. However, only the BCG/GM-DC group demonstrated a statistically significant reduction relative to the BCG group (Fig. 1**C**).

Since the adoptive transfer of DC subsets induced varying protective efficacy against Mtb infection during the early stage, we analyzed DCs and T cells of the lung, mediastinal lymph node (mLN), and spleen at 1 week after Mtb infection. DC and T cell **(Supplementary Fig. 2A)**, multifunctional T cells **(Supplementary Fig. 2B)**, and CD4$^+$ memory T cell subpopulations **(Supplementary Fig. 2C)** were analyzed according to the gating strategies. All groups that received different subsets of DCs showed an increase in lung DC numbers compared to the BCG group; however, only the BCG/GM-DC group showed an increased number of T cells in the lungs **(Supplementary Fig. 3A)**. Increased lung DCs were observed in each DC-transferred group, but only the BCG/GM-DC group exhibited increased DCs in mLN **(Supplementary Fig. 3A)**, indicating GM-DCs display greater migratory features. These results suggest that the adoptive transfer of GM-DC may increase the number and interaction of DCs with T cells in the mLN of BCG-immunized mice, thereby promoting rapid lung T cell accumulation. To confirm the signature of lung tissue by GM-DC transfer following BCG immunization, we analyzed RNA-seq data from lung tissues 1 week post-infection. GSEA revealed enrichment of gene sets related to T cell activation and chemokine signaling, highlighting coordinated immune cell recruitment in the BCG/GM-DC group (**Supplementary Fig. 3B, C**). The top 10 functional transcriptional changes in terms of gene ontology biological processes were analyzed by comparing with those from BCG-only vaccinated mice at 1 week after Mtb infection **(Supplementary Fig. 3D)**. As expected, the most significantly altered gene expression in the lungs of GM-DC-administered mice exhibited chemotaxis-associated genes such as *Cxcr3* and *Ccl20* (encoding a ligand of CCR6), which are engaged in T cell migration to the lung tissue **(Supplementary Fig. 3E)**. Protein-level validation confirmed that CCL17, CCL20, and CCL22 were also upregulated in the lungs of BCG/GM-DC mice, consistent with the RNA-seq findings (**Supplementary Fig. 3F**).

To examine Ag-specific T cell response that is recruited to the lungs during the early stage of infection, we evaluated the multifunctional properties of T cells producing IFN-γ, TNF-α, and IL-2 in response to PPD stimulation 1 week after the onset of infection (Fig. 1**D**). The groups that received FL-DC1, FL-DC2, and GM-DC exhibited higher levels of CD4$^+$ T cells that were positive for all three cytokines, IFN-γ, TNF-α, and IL-2, as well as those positive for two cytokines, IFN-γ and TNF-α or TNF-α and IL-2, when compared to the BCG-only group or the infection control group. Moreover, the BCG/GM-DC group exhibited a greater frequency of nearly all combinations of cytokine-producing CD4$^+$ T cells compared to the BCG/FL-DC1 and BCG/FL-DC2 groups (Fig. 1**D**). Whereas the profile of cytokine-producing CD8$^+$ T cell responses showed no statistical difference among groups. These results suggest that GM-DC

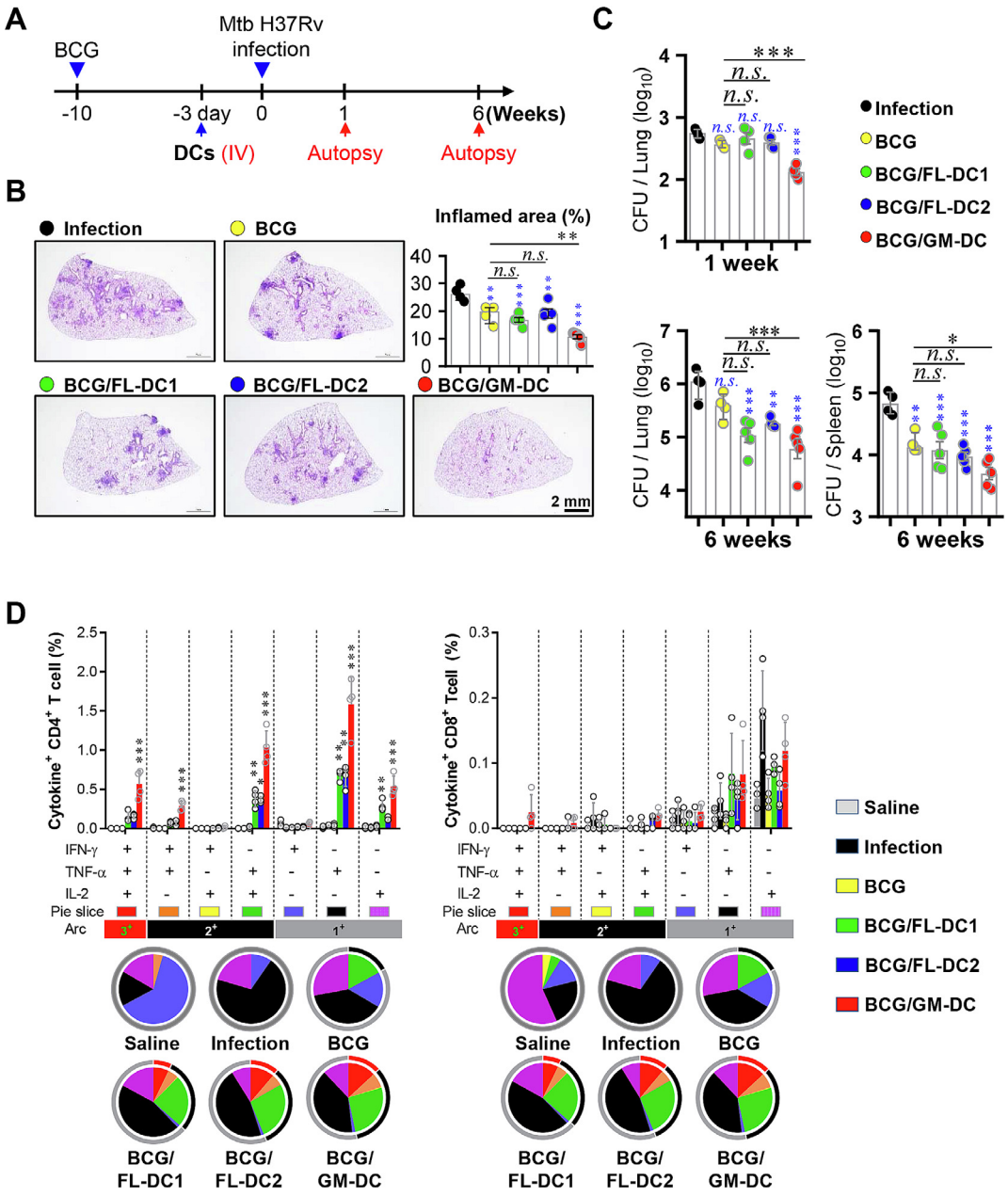

Fig. 1. Comparison of protective efficacy of various DC subsets against Mtb infection. (**A**) After 10 weeks from BCG vaccination, FL-DC1, FL-DC2, and GM-DC were transferred to BCG-immunized mice via an intravenous route. Three days later, the mice were infected with Mtb H37Rv (~130 CFUs/mouse). Mice were then sacrificed at 1 and 6 weeks post-infection. (**B**) Lung histopathology was analyzed using H&E at 6 weeks post-infection and (**C**) bacterial burdens in the lung at 1 week (upper panel) and in the lung and spleen at 6 weeks post-infection (lower panel) were assessed. $n = 3–5$. Blue asterisk without designation indicates comparison to infection group. (**D**) One week after the Mtb H37Rv challenge, PPD-specific lung $CD4^+$ T cells producing the indicated cytokines were analyzed. $n = 4$. Statistical analysis was performed by one-way ANOVA with Tukey's multiple comparisons. $^*p < 0.05$, $^{**}p < 0.01$, and $^{***}p < 0.001$. Asterisk without designation indicates comparison to BCG group. The mean frequencies of cells co-producing IFN-γ, TNF-α, and/or IL-2 are represented in the pie charts. The arcs surrounding the pie charts denote the number of cytokines produced by the T cells. Data are mean ± SD. FL-DC1: FLT3 ligand-derived $CD11b^+$ BMDCs matured with CFA, FL-DC2: FLT3 ligand-derived $CD11b^-$ BMDCs matured with CFA: GM-DC: GM-CSF derived BMDCs matured with CFA. (For interpretation of the references to colour in this figure legend, the reader is referred to the web version of this article.)

administration, compared to FL-DCs, more effectively recruits T cells and DCs to the lungs and mLNs following BCG vaccination, while also better promoting the induction of protective multifunctional $CD4^+$ Th1 cells in lung tissue, leading to superior protection during the early stage of Mtb infection.

Next, we examined whether the enhanced protection of the BCG/GM-DC group was dependent on GM-DC number, and whether it was mediated by an Mtb Ag-specific response. The BCG boosting effect was evaluated by administering either a low dose of 1×10^5 cells per mouse or a high dose of 1×10^6 cells per mouse of GM-DC transfer according to the specified experimental schedule **(Supplementary Fig. 4A)**. The BCG/GM-DC group exhibited a decrease in inflammatory lesions and lung bacterial growth, correlating with the number of transferred GM-DCs **(Supplementary Fig. 4B, C)**. We then conducted an experiment to investigate whether the enhanced protection of the BCG with GM-DC transfer was due to DC maturation status or specificity to the Mtb-Ag. We adoptively transferred immature GM-DC (imGM-DC), matured DC with a Toll-like receptor 2 agonist, Pam3 (Pam3-GM-DC), or Mtb-Ag-matured GM-DC into BCG-vaccinated mice **(Supplementary Fig. 4D)**. Although the BCG/imGM-DC and BCG/Pam3-GM-DC groups showed no additional reduction in the lung pathological

severity **(Supplementary Fig. 4E)** or the bacterial growth in the lung and spleen **(Supplementary Fig. 4F)** compared to the BCG group, the BCG/GM-DC group demonstrated superior protective efficacy over all other tested groups, indicating that the enhanced protection conferred by the BCG/GM-DC group depends on the number of transferred GM-DCs in an Mtb-Ag-specific manner. This demonstrates that GM-DC transfer enhances the vaccine efficacy of the BCG through an Mtb Ag-specific immune response.

GM-DC transfer enhances BCG vaccine efficacy against various Mtb clinical strains by expanding preexisting Th1 responses

BCG vaccine efficacy varies depending on the Mtb strains [16]. To determine whether the enhanced protection provided by BCG/GM-DC against the virulent H37Rv strain is applicable to clinical Mtb isolates, we infected mice with Erdman, HN878, and Mtb K strains (Fig. 2**A**). The BCG/GM-DC group showed reduced bacterial

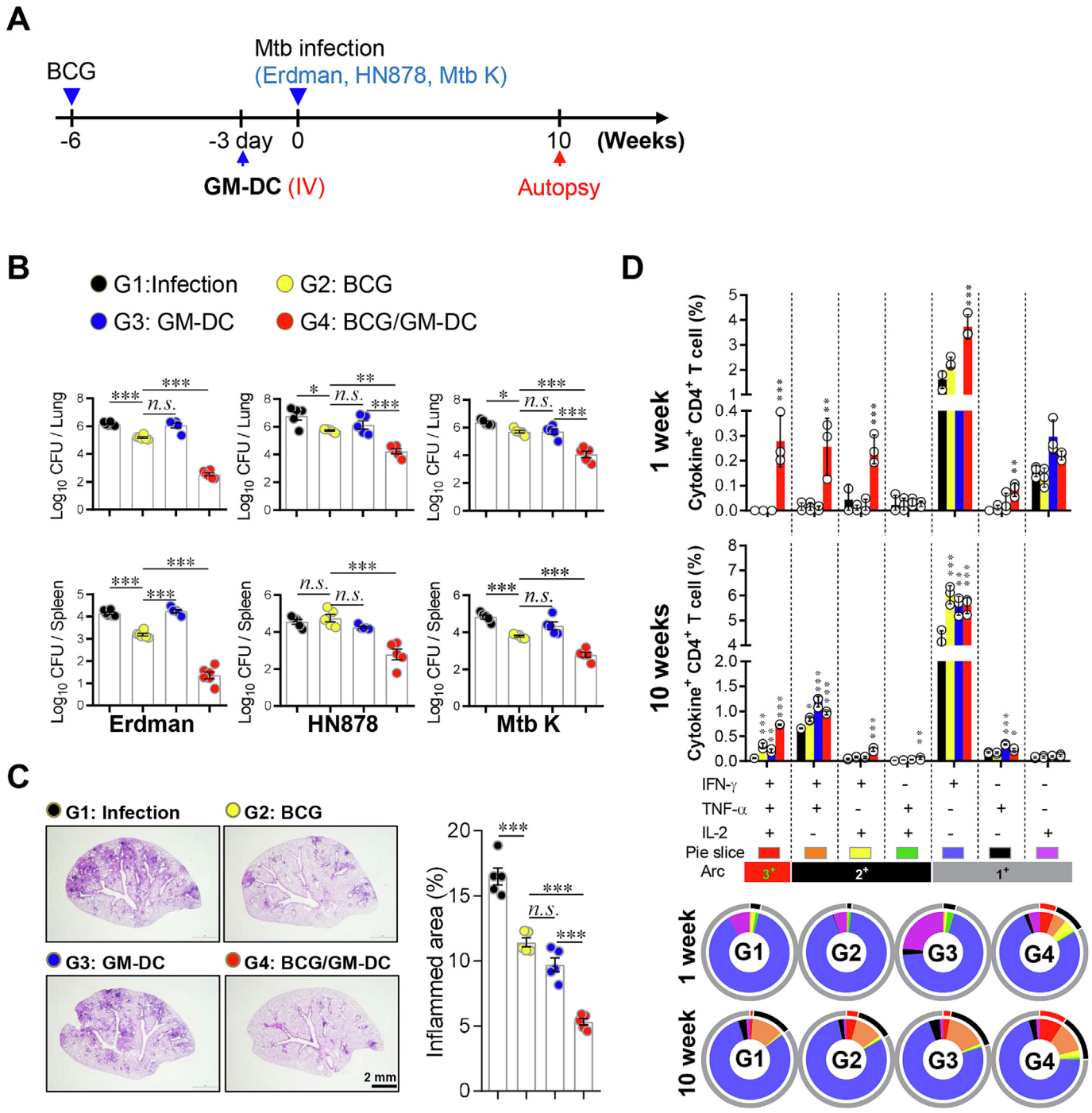

Fig. 2. Protective efficacy of GM-DC transfer after BCG vaccination against various Mtb clinical strains in mice. (**A**) After 6 weeks from BCG vaccination, GM-DC were transferred to non-vaccinated or BCG-immunized mice via an intravenous route. Mice were challenged with HN878, Erdman, or K strain (~200 CFUs/mouse, each strain). (**B**) After 10 weeks from challenge, mice from each group were sacrificed and bacterial growth of lung and spleen were evaluated. $n = 5–6$. (**C**) After 10 weeks from challenge with Mtb K, the superior lobes of the right lung were analyzed using H&E staining, and the inflamed areas were presented as dot graph. $n = 5$. (**D**) One week and ten weeks after the Mtb K challenge, PPD-specific lung $CD4^+$ T cells producing the indicated cytokines were analyzed. $n = 3$. The mean frequencies of cells co-producing IFN-γ, TNF-α, and/or IL-2 are represented in the pie charts. The arcs surrounding the pie charts denote the number of cytokines produced by the T cells. Data are mean ± SD. Statistical analysis was performed by one-way ANOVA with Tukey's multiple comparisons. $^*p < 0.05$, $^{**}p < 0.01$, and $^{***}p < 0.001$. Asterisk without designation indicates comparison to BCG group. GM-DC, CFA-matured DC differentiated with GM-CSF.

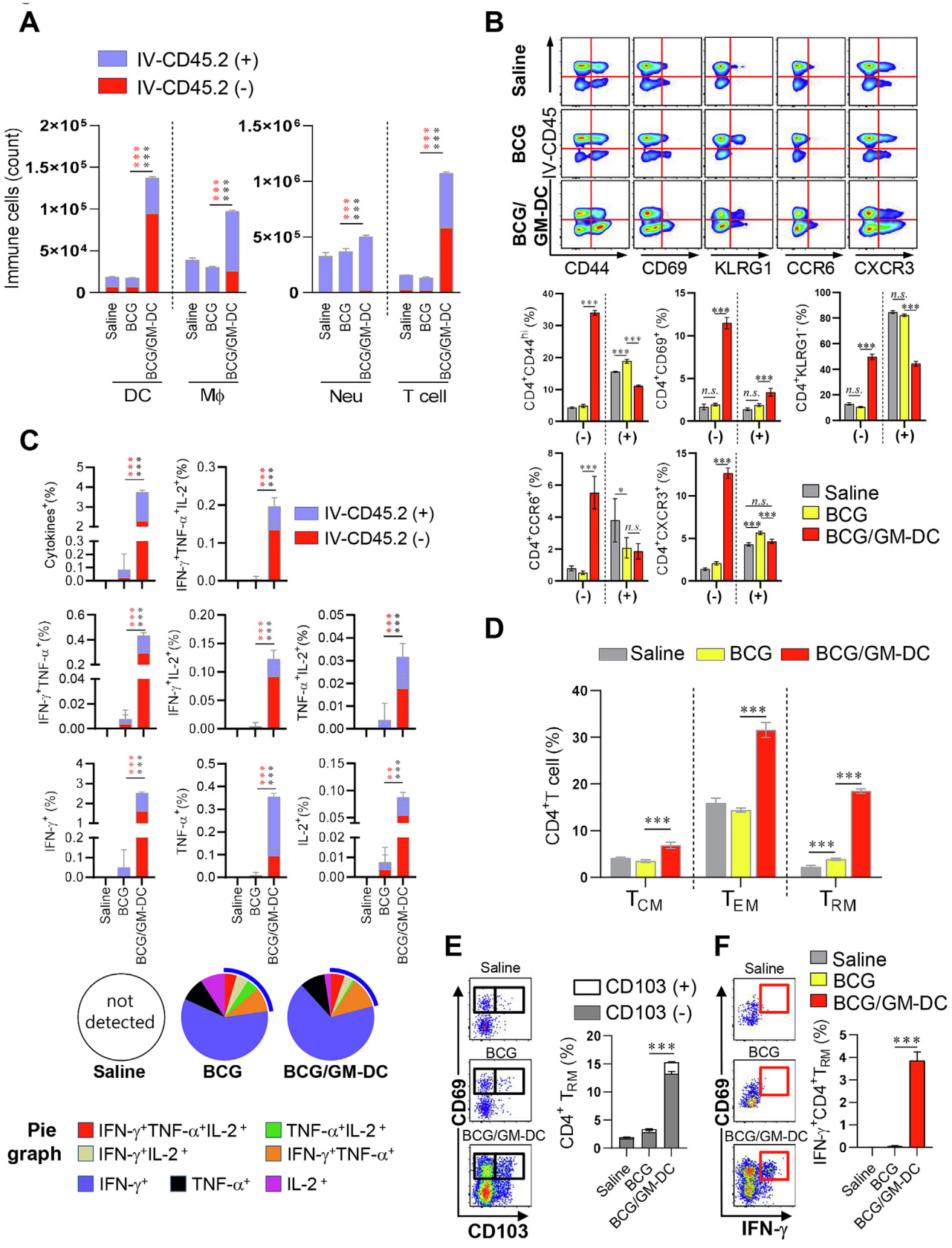
A
IV-CD45.2 (+)
IV-CD45.2 (-)
Immune cells (count)
DC
Mϕ
Neu
T cell
Saline
BCG
BCG/GM-DC
B
Saline
BCG
BCG/GM-DC
IV-CD45
CD44
CD69
KLRG1
CCR6
CXCR3
C
Cytokines+(%)
IFN-γ+TNF-α+IL-2+(%)
IFN-γ+TNF-α+(%)
IFN-γ+IL-2+(%)
TNF-α+IL-2+(%)
IFN-γ+(%)
TNF-α+(%)
IL-2+(%)
not detected
Saline
BCG
BCG/GM-DC
Pie graph
IFN-γ+TNF-α+IL-2+
TNF-α+IL-2+
IFN-γ+IL-2+
IFN-γ+TNF-α+
IFN-γ+
TNF-α+
IL-2+
D
CD4+T cell (%)
TCM
TEM
TRM
E
CD69
CD103
CD103 (+)
CD103 (-)
CD4+ TRM (%)
F
IFN-γ
IFN-γ+CD4+TRM (%)

growth against all tested Mtb strains at 10 weeks post-infection, whereas no significant effect was observed in the GM-DC-alone group in the absence of BCG vaccination (**Fig. 2B**), indicating that GM-DC boosts preexisting immune response established by the BCG vaccination. Consistent with CFU reductions, the BCG/GM-DC group exhibited the smallest inflamed area (**Fig. 2C**). Immunohistochemical staining was conducted to quantify the major cellular composition of granulomas, including neutrophils, macrophages, T cells, and B cells, across experimental groups. Consistent with the analysis of inflamed areas, the BCG/GM-DC group exhibited the lowest levels of all immune cell populations (**Supplementary Fig. 5A**) as well as less extensive fibrotic regions (**Supplementary Fig. 5B**).

Next, to investigate lung Ag-specific $CD4^+$ T cell responses, we measured $CD4^+$ T cell co-producing IFN-γ, TNF-α, and IL-2 following PPD stimulation at 1 and 10 weeks post-infection (**Fig. 2D**). Because the average lung CFU reductions of BCG vaccine against Erdman, HN878, and Mtb K infection were 0.9629 $\log_{10}$, 1.053 $\log_{10}$, and 0.6698 $\log_{10}$, respectively, hereafter, Mtb K, which showed the lowest BCG vaccine efficacy, was used for subsequent experiments (**Fig. 2B**). Similar to results with Mtb H37Rv infection (**Fig. 1D**), the $CD4^+$ multifunctional T cells (triple- and double-positive cytokines) were increased in the BCG/GM-DC group 1 week post-Mtb K infection (**Fig. 2D, upper panel**). Ten weeks post-infection, the multifunctional $CD4^+$ T cells producing triple cytokines were increased in BCG/GM-DC group (**Fig. 2D, lower panel**). In addition, the increase in multifunctional $CD4^+$ T cell response at 1 week after Mtb K strain infection was not found in the group that received only GM-DC transfer without BCG. These results indicate that the adoptive transfer of GM-DC enhances the protective vaccine efficacy of the BCG against several Mtb strains by inducing early Th1 responses and boosting preexisting BCG immunity.

GM-DC enhances preexisting Ag-specific memory T cell responses established by BCG vaccination in the lung parenchyma prior to Mtb infection

Vaccination-induced memory T cells facilitate a prompt and protective response of T cells against Mtb infection. As Mtb is a respiratory pathogen, lung-resident memory T cell (T_{RM}) formation may facilitate an immediate T cell response [36]. Since we observed an increase in Ag-specific T cell responses in the lung at early phase of Mtb infection by GM-DC transfer after BCG vaccination, we analyzed lung tissue, mLN, and spleen to investigate whether GM-DC transfer alters BCG-induced preexisting immune responses prior to Mtb infection. Since the expression of genes related to mucosal homing and parenchymal localization was already elevated in the first week of infection (**Supplementary Fig. 3C**), we confirmed the composition and parenchymal localization of immune cells prior to Mtb infection using IV staining with anti-CD45 antibody (**Fig. 3A**). As a result, the BCG/GM-DC group exhibited a greater number of DCs and T cells compared to the BCG-alone group and, in particular, a significant number of cells were localized within the lung parenchyma (**Fig. 3A**). Lung parenchyma-residing T cells have been reported to provide greater protection against Mtb infection than those confined to the vasculature [37]. In this study, the BCG/GM-DC group showed prominent localization of T cells to the lung parenchyma. Therefore, we analyzed the molecules related to the functional phenotypic differences (CD44, KLRG1) and lung chemotactic localization (CCR6, CXCR3, CD69) of T cells located in the vascular and parenchymal regions (**Fig. 3B**). The BCG/GM-DC group exhibited a higher prevalence of $CD44^{hi}CD4^+$ T cells in the lung parenchyma compared to the BCG group. Additionally, CD69, associated with tissue retention, and the chemokine receptors CCR6 and CXCR3, were more frequently expressed by $CD4^+$ T cells in the parenchyma of the BCG/GM-DC group than in the BCG group. In the lung parenchymal region, $KLRG1^-CD4^+$ T cells were more abundant in the BCG/GM-DC group than in the BCG group, whereas their frequency in the vascular region was lower than in the BCG group (**Fig. 3B**). $CD8^+$ T cells showed a pattern analogous to that observed in $CD4^+$ T cells (**Supplementary Fig. 6A**).

Next, we analyzed PPD-induced multifunctional T cell responses to assess differences in vascular and parenchymal T cell function following GM-DC adoptive transfer. In the BCG/GM-DC group, $CD4^+$ T cells producing IFN-γ, TNF-α, and/or IL-2 were present at higher frequencies in both the parenchyma and vascular compartments than in the BCG group (**Fig. 3C, Supplementary Fig. 6B**). In addition, despite similar proportions of multiple-cytokine-producing $CD4^+$ T cells in the pie graph between the BCG/GM-DC and BCG groups, the actual frequencies of these cells were higher in the BCG/GM-DC group than in the BCG group (**Fig. 3C**). The pattern of cytokine production by $CD8^+$ T cells was similar to that of $CD4^+$ T cells, showing a higher frequency in the lung parenchymal region of the BCG/GM-DC group compared to the BCG group. However, cytokine-producing $CD8^+$ T cells were observed at lower frequencies than $CD4^+$ T cells across most combinations of cytokines (**Supplementary Fig. 6C**). Furthermore, consistent with the results observed in the lung, the BCG/GM-DC group exhibited higher numbers of DCs and T cells in the mLN and spleen compared to the BCG group, with this trend being more pronounced in the mLN (**Supplementary Fig. 7A**). For PPD-specific T cell responses, $CD4^+$ T cells exhibited greater reactivity to PPD stimulation than $CD8^+$ T cells in the mLN and spleen (**Supplementary Fig. 7B**).

Given the potent $CD4^+$ memory T cell responses observed in the BCG/GM-DC group following PPD stimulation, we analyzed whether GM-DC adoptive transfer altered $CD4^+$ memory T cell subpopulations in the BCG-vaccinated group (**Fig. 3D**). $CD4^+$ memory T cell subpopulations were analyzed based on the gating strategies (**Supplementary Fig. 2C**). The BCG/GM-DC group exhibited increased frequencies of central memory T cells (T_{CM}), effector memory T cells (T_{EM}), and T_{RM} in the lungs compared to the BCG group, especially in T_{RM} (**Fig. 3D**). CD103 is considered one of the markers of T_{RM}, but in many cases, the $CD4^+$ T_{RM} population does not express CD103 [38]. Therefore, we examined CD103 expression

Fig. 3. Analysis of $CD4^+$ T cell response in the lungs of BCG-immunized mice after GM-DC transfer. GM-DC was transferred after 10 weeks from BCG vaccination. After 3 days, mice were sacrificed for analysis. (**A**) The localization of lung immune cells in vascular or parenchymal regions were analyzed. $n = 4$. (**B**) The localization of lung $CD4^+$ T cells was analyzed according to the expression of CD44, CD69, KLRG1, CCR6, and CXCR3. $n = 4$. (**C**) PPD-specific $CD4^+$ T cells producing multiple cytokines in the lung parenchymal and vascular areas were examined. The mean frequencies of cells co-producing IFN-γ, TNF-α, and/or IL-2 are represented in the pie charts. The arcs surrounding the pie charts indicate the $CD4^+$ T cells that produce multiple cytokines. $n = 4$. (**D**) The effect of GM-DC transfer on the formation of memory type of $CD4^+$ T cells (T_{CM}, T_{EM}, and T_{RM}) in the lung were analyzed. To further analyze the lung $CD4^+$ T_{RM} population, (**E**) the expression of CD103 and (**F**) IFN-γ production of T_{RM} in response to PPD stimulation were analyzed. $n = 4$. Data are mean ± SD. Statistical analysis was performed by one-way ANOVA with Tukey's multiple comparisons. *n.s.* = not significant, $^*p < 0.05$, $^{**}p < 0.01$, and $^{***}p < 0.001$. Comparison between IV-CD45.2(−) value: red asterisk, comparison between total value: black asterisk. DC, dendritic cell: MΦ, macrophage: Neu, neutrophil: Resident memory T cell, T_{RM}: effector memory T cell, T_{EM}: Central memory T cell, T_{CM}. (For interpretation of the references to colour in this figure legend, the reader is referred to the web version of this article.)

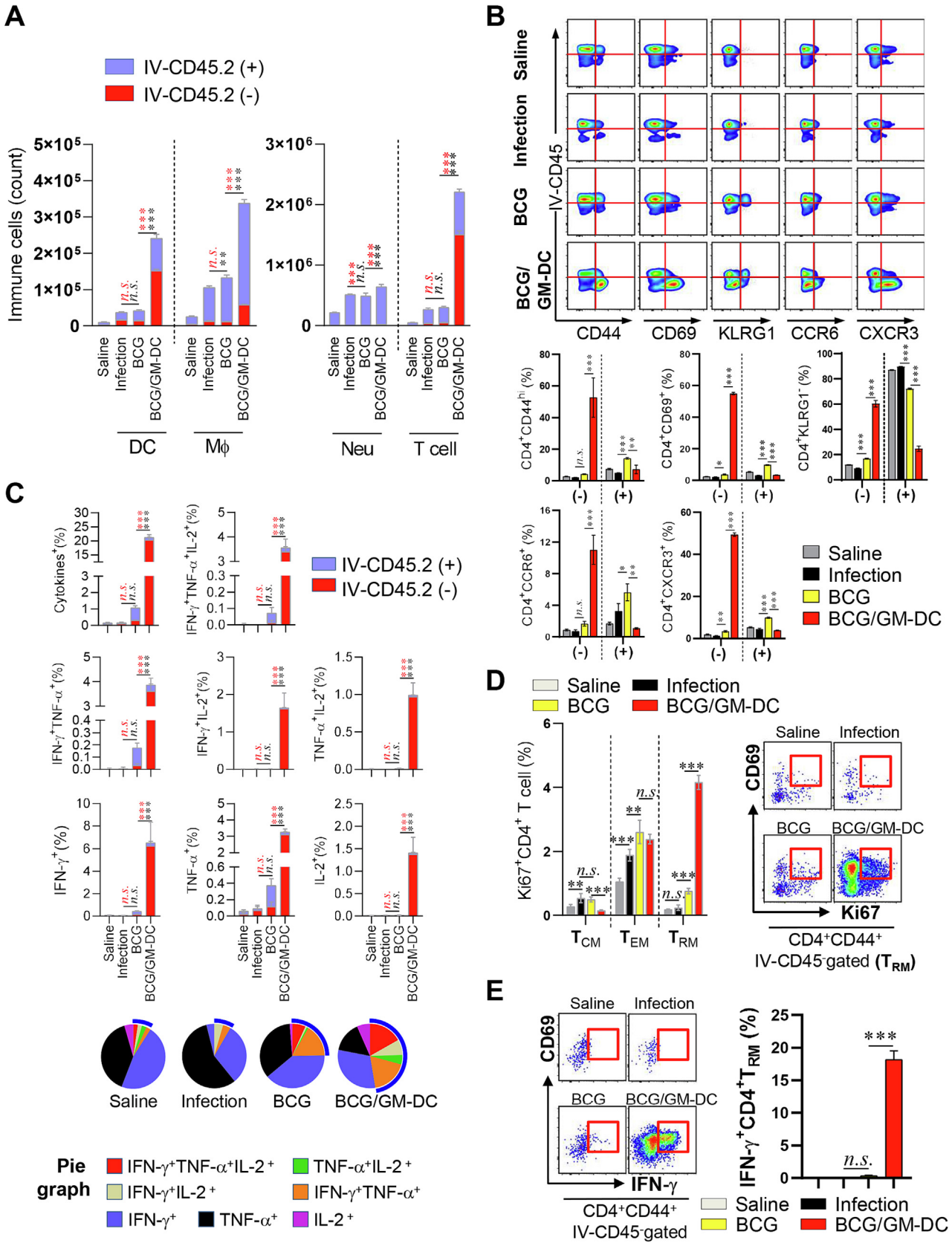
A
IV-CD45.2 (+)
IV-CD45.2 (-)
Immune cells (count)
Saline
Infection
BCG
BCG/GM-DC
DC
Mϕ
Neu
T cell
B
IV-CD45
CD44
CD69
KLRG1
CCR6
CXCR3
Saline
Infection
BCG
BCG/GM-DC
C
Cytokines+(%)
IFN-γ+TNF-α+IL-2+(%)
IFN-γ+TNF-α+(%)
IFN-γ+IL-2+(%)
TNF-α+IL-2+(%)
IFN-γ+(%)
TNF-α+(%)
IL-2+(%)
Pie graph
IFN-γ+TNF-α+IL-2+
TNF-α+IL-2+
IFN-γ+IL-2+
IFN-γ+TNF-α+
IFN-γ+
TNF-α+
IL-2+
D
Ki67+CD4+ T cell (%)
TCM
TEM
TRM
CD69
Ki67
CD4+CD44+
IV-CD45-gated (TRM)
E
IFN-γ+CD4+TRM (%)
IFN-γ
CD4+CD44+
IV-CD45-gated

on $CD4^+$ T_{RM} in the lungs of vaccinated mice. As a result, the majority of $CD4^+$ lung T_{RM} induced by GM-DC transfer did not express CD103 (Fig. 3**E**). To confirm the Ag specificity of this memory T cell population, we analyzed IFN-γ-producing $CD4^+$ T_{RM} following PPD stimulation. This population was scarcely detected in the BCG group but was present exclusively in the BCG/GM-DC group (Fig. 3**F**). These results suggest that the adoptive transfer of GM-DCs enhances BCG-induced immunity by increasing lung-resident $CD4^+$ $T_{RM,}$ followed by the expansion of multifunctional T cells, particularly in the lung parenchyma.

GM-DC induces a rapid T cell response in the lung parenchyma of BCG-vaccinated mice after Mtb infection

Since T cell localization to the parenchyma was confirmed prior to Mtb infection following GM-DC transfer in the lungs of BCG-immunized mice, and protective efficacy was observed through bacterial burden control at 1 week post-infection (Fig. 1**C**), we sought to determine the early T cell response based on localization at 1 week after Mtb infection. Similar to the results for H37Rv infection, the BCG/GM-DC group also showed a lower lung bacterial burden in Mtb K infection than the BCG group at 1 week post-infection (**Supplementary Fig. 8A**). The BCG group displayed similar levels of immune cell infiltration as the infection control group, while the BCG/GM-DC group demonstrated heightened infiltration of DCs, macrophages, and T cells (Fig. 4**A**). Moreover, T cells of the BCG/GM-DC group were localized at a higher proportion in the parenchymal region compared to their distribution before Mtb infection (Fig. 4**A**). In the BCG/GM-DC group, the frequency of $CD44^{hi}CD4^+$ T cells was higher than in the infection control and BCG group in the lung parenchyma. $CD69^+CD4^+$ T cells, $CCR6^+CD4^+$ T cells, $CXCR3^+CD4^+$ T cells, and $KLRG1^-CD4^+$ T cells were more abundant in the parenchymal region and less frequent in the vascular region compared to the infection and BCG groups (Fig. 4**B**). $CD8^+$ T cells exhibited a similar pattern to $CD4^+$ T cells (**Supplementary Fig. 8B**). These results suggest that the administration of GM-DCs to BCG-immunized mice accelerates lung parenchymal localization of $CD4^+$ T cells with an activated and protective phenotype.

Next, we analyzed multifunctional T cell responses to confirm the functionality of these parenchymal and vascular T cells. The BCG-immunized group demonstrated a slight increase in the frequency of $CD4^+$ T cells producing IFN-γ, TNF-α, and/or IL-2 in response to PPD stimulation, with the majority of these cells localized within the vascular regions (Fig. 4**C**). In the BCG/GM-DC group, $CD4^+$ T cells producing most combinations of cytokines were more frequent than in the BCG group and were primarily localized within the lung parenchyma. Furthermore, the proportion of multifunctional T cells was greater in comparison to the BCG and infection group (Fig. 4**C, Supplementary Fig. 8C**). IFN-γ, TNF-α, and/or IL-2 producing $CD8^+$ T cells were more frequent in the BCG/GM-DC group than in the BCG group, with the majority of these cytokine-producing $CD8^+$ T cells localized within the parenchyma. $CD8^+$ T cells exhibited similar cytokine production patterns to $CD4^+$ T cells, though at a lower frequency (**Supplementary Fig. 8D**). The BCG/GM-DC group exhibited increased numbers of DCs and T cells in the mLN and spleen compared to the BCG group (**Supplementary Fig. 9A**). In the mLN and spleen, the BCG/GM-DC group exhibited an increase in PPD-specific multifunctional $CD4^+$ T cells, while the frequency of multifunctional $CD8^+$ T cells remained comparable between the groups (**Supplementary Fig. 9B**). These findings suggest that the adoptive transfer of GM-DC into BCG-immunized mice predominantly triggers a potent $CD4^+$ T cell response over a $CD8^+$ T cell response during the initial infection phase. Next, we assessed $CD4^+$ memory T cell subsets expressing the proliferation marker Ki67 to evaluate the early responsiveness of vaccine-induced memory T cells to Mtb infection. In alignment with the $CD4^+$ T cell response to PPD stimulation, the BCG/GM-DC group exhibited a significantly elevated frequency of $Ki67^+$ T_{RM} cells localized within the lung parenchyma compared to the BCG group (Fig. 4**D**). Moreover, IFN-γ-producing $CD4^+$ T_{RM} cells in response to PPD stimulation were scarcely detected in the BCG and infection control group, whereas their presence was exclusively observed in the BCG/GM-DC group (Fig. 4**E**). One week post-infection, the BCG/GM-DC group showed higher *Ccl20* expression in the lung tissue and a greater frequency of CCR6-expressing $CD4^+$ T cells than the BCG group (**Supplementary Fig. 3C,** Fig. 4**B**). CCR6 is a surface marker of Th17 cells involved in playing a protective role in the early stages of Mtb infection [39]. Therefore, we examined IL-17A-producing $CD4^+$ T cells in lung tissue following GM-DC administration after BCG vaccination. IL-17A-producing $CD4^+$ T cells were not detected in lung tissue prior to infection (**Supplementary Fig. 10A**). However, 1 week post-infection, the BCG/GM-DC group showed a higher frequency of IL-$17A^+$ $CD4^+$ T cells compared to the BCG group. Most of these cells were localized to the IV-$CD45^-$ lung parenchyma (**Supplementary Fig. 10B**). A previous study has demonstrated that Th17 cells facilitate the recruitment of optimal Th1 cells [40], suggesting that the Th17 responses induced by GM-DC administration could support the robust Th1 response observed at 1 week post-infection. Collectively, these results suggest that administering GM-DCs to mice immunized with BCG enhances the rapid activation of protective T cell responses within the parenchymal region during the early stage of Mtb infection.

Next, we investigated T cell responses at a late phase of infection. Firstly, similar to the prior result (Fig. 2**B**), the BCG/GM-DC group also showed a lower bacterial burden of lung and spleen than the BCG group at 6 week post-infection (**Supplementary Fig. 11A**). Since $CD4^+$ T cell cytokine profiles and phenotypes associated with control of Mtb chronic infection [41], we analyzed the PPD-specific multifunctional T cell response to evaluate the protective immune response elicited by BCG/GM-DC. As a result, IL-2 producing $CD4^+$ T cells across all cytokine combinations exhibited the highest frequency in the BCG/GM-DC group (**Supplementary**

Fig. 4. Analysis of $CD4^+$ T cell response in the lung of GM-DC-transferred mice after BCG vaccination at 1 week post Mtb infection. After 10 weeks from BCG vaccination, GM-DC was transferred to BCG-immunized mice. Three days later, mice were infected with the Mtb strain K (~250 CFUs/mouse). (**A**) One week post-infection, the localization of lung immune cells in vascular and parenchymal regions were analyzed. $n = 4$. (**B**) The localization of $CD4^+$ T cells in the lungs was analyzed based on the expression of CD44, CD69, KLRG1, CCR6, and CXCR3. $n = 4$. (**C**) PPD-specific $CD4^+$ T cells producing multiple cytokines in the lung parenchymal and vascular areas were examined. The mean frequencies of cells co-producing IFN-γ, TNF-α, and/or IL-2 are represented in the pie charts. The arcs surrounding the pie charts indicate the $CD4^+$ T cells that produce multiple cytokines. $n = 4$. (**D**) The expression of Ki67 of memory type of $CD4^+$ T cells in the lung were analyzed. The dot plots represent $Ki67^+$ T_{RM} in the lung of each group. $n = 4$. (**E**) PPD-specific $CD4^+$ T_{RM} in lung producing IFN-γ were measured. $n = 4$. Data are mean ± SD. Statistical analysis was performed by one-way ANOVA with Tukey's multiple comparisons. *n.s.* = not significant, $^*p < 0.05$, $^{**}p < 0.01$, and $^{***}p < 0.001$. Comparison between IV-CD45.2(−) value: red asterisk, comparison between total value: black asterisk. DC, dendritic cell: MΦ, macrophage: Neu, neutrophil: Resident memory T cell, T_{RM}: effector memory T cell, $T_{EM:}$ Central memory T cell, T_{CM}. (For interpretation of the references to colour in this figure legend, the reader is referred to the web version of this article.)

Fig. 11B). IL-2 serves as a pivotal cytokine that plays a crucial role in the survival and proliferation of T cells, while CD127 and KLRG1 expression correlates with the lifespan and functionality of $CD4^+$ T cells [41,42]. Therefore, we analyzed the expression of KLRG1 and CD127, markers of T cell differentiation and lifespan, and Ki67, a proliferation marker, in lung $CD4^+$ T cells **(Supplementary Fig. 11C)**. The BCG/GM-DC group exhibited the highest frequency of $CD44^{hi}CD127^+KLRG1^-CD4^+$ T cells, while the $CD44^{hi}CD127^-KLRG1^+CD4^+$ T cells exhibited the lowest frequency among all groups, regardless of localization **(Supplementary Fig. 11D)**. $Ki67^+KLRG1^-CD44^{hi}CD4^+$ T cells also showed the highest frequency in the parenchymal region of the BCG/GM-DC group, whereas $CD44^{hi}Ki67^+KLRG1^-CD4^+$ T cells showed the lowest frequency in the vascular region of the BCG/GM-DC group **(Supplementary Fig. 11D)**. These results indicate that adoptive transfer of GM-DCs sustains protective responses by maintaining the proliferation of protective $CD4^+$ T cells during the late stages of Mtb infection in BCG-immunized mice.

GM-DC transfer reinforced waning effect of BCG vaccine resulting in long-lasting protective immunity against Mtb infection

One of the problems with the BCG vaccine is its waning efficacy over time [2]. Given our confirmation of enhanced protective $CD4^+$ T cell responses and improved vaccine efficacy against Mtb through GM-DC transfer to BCG-immunized mice, we investigated whether the immunogenicity and vaccine efficacy induced by BCG/GM-DC vaccination were sustained over an extended period. Six weeks after BCG vaccination, GM-DCs were administered, and the mice were euthanized at 32 weeks from BCG vaccination **(**Fig. 5**A)**. The BCG/GM-DC group sustained a stronger Ag-specific multifunctional $CD4^+$ T cell response than the BCG group **(**Fig. 5**B)**. Ten weeks post-infection with Mtb K, the BCG/GM-DC group exhibited less severe lung inflamed regions **(**Fig. 5**C)** and a lower bacterial burden **(**Fig. 5**D)** than the BCG group. The efficacy of the BCG vaccine declines over time, which may be associated with T cell exhaustion that impairs T cell functions [43]. To assess whether GM-DC administration influences T cell exhaustion on BCG-vaccinated mice, we analyzed the co-expression of exhaustion markers Tim-3 and PD-1 on lung T cells at 10 weeks post-infection. Interestingly, lower $Tim\text{-}3^+PD\text{-}1^+$ T cells were detected in the lungs of the BCG/GM-DC group compared to the BCG group **(Supplementary Fig. 12A)**. Consistently, according to the experimental schedule shown in Fig. 1, we also confirmed that the frequency of $Tim\text{-}3^+PD\text{-}1^+$ $CD4^+$ T cells was lower in the BCG/GM-DC group than in the BCG group at 6 weeks post-infection **(Supplementary Fig. 12B)**. These results indicate that GM-DC transfer augments BCG-induced T cell immunity with less exhaustion, enhancing the anti-TB vaccine efficacy of BCG, which declines over time. Next, to evaluate the age-dependent effect of the GM-DC boosting strategy, we administered GM-DCs at 30 weeks after BCG vaccination and assessed the efficacy of the BCG/GM-DC vaccine strategy (**Supplementary Fig. 13A**). Ten weeks post-infection with Mtb K, the BCG/GM-DC group exhibited less severe lung inflamed regions **(Supplementary Fig. 13B)** and a lower bacterial burden **(Supplementary Fig. 13C)** than the BCG group, suggesting that the DC-based boosting strategy enables the restoration or enhancement of protective immunity even after a long delay following BCG vaccination.

GM-DC transfer presented a long-lasting protection on BCG vaccination against low dose and lethal dose Mtb infection

Next, the efficacy of BCG/GM-DC was evaluated in a low dose Mtb infection model. The physiological infection environment of human TB is closely resembled by the low dose aerosol Mtb infection model [44]. In this study, mice were infected via aerosol with Mtb at a dose of approximately 10 CFUs per mouse, which is sufficient to infect all mice. After the vaccination, the Mtb K strain was challenged via aerosol route, and mice were sacrificed 2, 4, 8, and 16 weeks post-infection for bacterial growth and histopathology analysis (Fig. 6**A**). The BCG-vaccinated group showed a 1 $\log_{10}$ reduction in bacterial burden across all time points, whereas GM-DC transfer resulted in a 3–4 $\log_{10}$ reduction throughout the monitored period **(**Fig. 6**B)**. Particularly, no bacteria were detected in the BCG/GM-DC group at 2 weeks post-infection, and from 4 to 16 weeks, only one mouse showed detectable Mtb growth. Consistent with the bacterial burden results, lung inflamed lesions started to form and grew over time, whereas the BCG/GM-DC group showed only minimal inflamed lesions at all analysis timepoints **(**Fig. 6**C)**. Major immune cells consisting of Mtb-induced granulomas and fibrotic regions were analyzed by immunohistochemical staining and Sirius Red staining at 8 and 16 weeks post-infection. At 8 weeks post-infection, no notable differences in immune cell composition were observed across the groups **(Supplementary Fig. 14A)**. At 16 weeks post-infection, neutrophils and macrophages were found at the lowest levels in the BCG/GM-DC group, while the extent of fibrosis appeared comparable across the groups **(Supplementary Fig. 14B)**.

Next, we explored the maximal efficacy of the BCG/GM-DC against Mtb K strain challenge at a high dose causing lethal outcome. First, a high dose challenge model was conducted according to the indicated time points **(**Fig. 6**D)**. Nineteen to twenty days after the challenge, all unvaccinated mice succumbed **(**Fig. 6**E)**. The BCG-vaccinated group and BCG/imGM-DC group began succumbing at 26 days post-infection, and all remaining mice in these two groups had died by approximately 40 days post-infection. In contrast, the BCG/GM-DC group maintained a 100 % survival rate until 96 days post-infection **(**Fig. 6**E)**. Three weeks post-challenge (infection group) or four weeks post-challenge (BCG, BCG/imGM-DC), lung histopathology was analyzed. Uncontrolled inflammation was observed, whereas the BCG/GM-DC group exhibited well-controlled granulomas at 14 weeks post-infection **(**Fig. 6**F)**. These results indicate that GM-DC enhances the efficacy of BCG vaccination, irrespective of the infection dose.

Therapeutic intervention with GM-DC during antibiotic treatment reduced bacterial CFUs and lung inflammation by eliciting potent Th1 immune responses

Achieving effective TB control requires a multifaceted strategy, integrating the treatment of TB patients with preventive measures, while emphasizing the reduction of treatment durations and relapse rates to improve treatment outcomes and disease management overall. We investigated whether GM-DC administration could enhance the efficacy of an immunotherapeutic vaccine and reduce treatment duration. To investigate the potential of this strategy in improving treatment outcomes, we evaluated the efficacy of antibiotics (INH + RIF, Abx) combined with GM-DC or imGM-DC administration, starting at 4 weeks post-infection when the bacterial burden peaks **(**Fig. 7**A)**. We verified that the therapy successfully suppressed bacterial growth in the lungs at both the start and end points of Abx treatment **(**Fig. 7**B).** At 12 weeks post-infection, the bacterial burden in the lungs and spleen was lower in the group treated with antibiotics combined with GM-DC injection (Abx + GM-DC) compared to the antibiotics-only group (Abx). The Abx + GM-DC group achieved an additional reduction of 1.514 $\log_{10}$ CFUs in the lungs and 1.676 $\log_{10}$ CFUs in the spleen relative to the Abx group **(**Fig. 7**C).** In contrast, consistent with the results of GM-DC administration as a BCG booster vaccine, the imGM-DC group combined with antibiotics (Abx + imGM-DC) showed no additional therapeutic efficacy

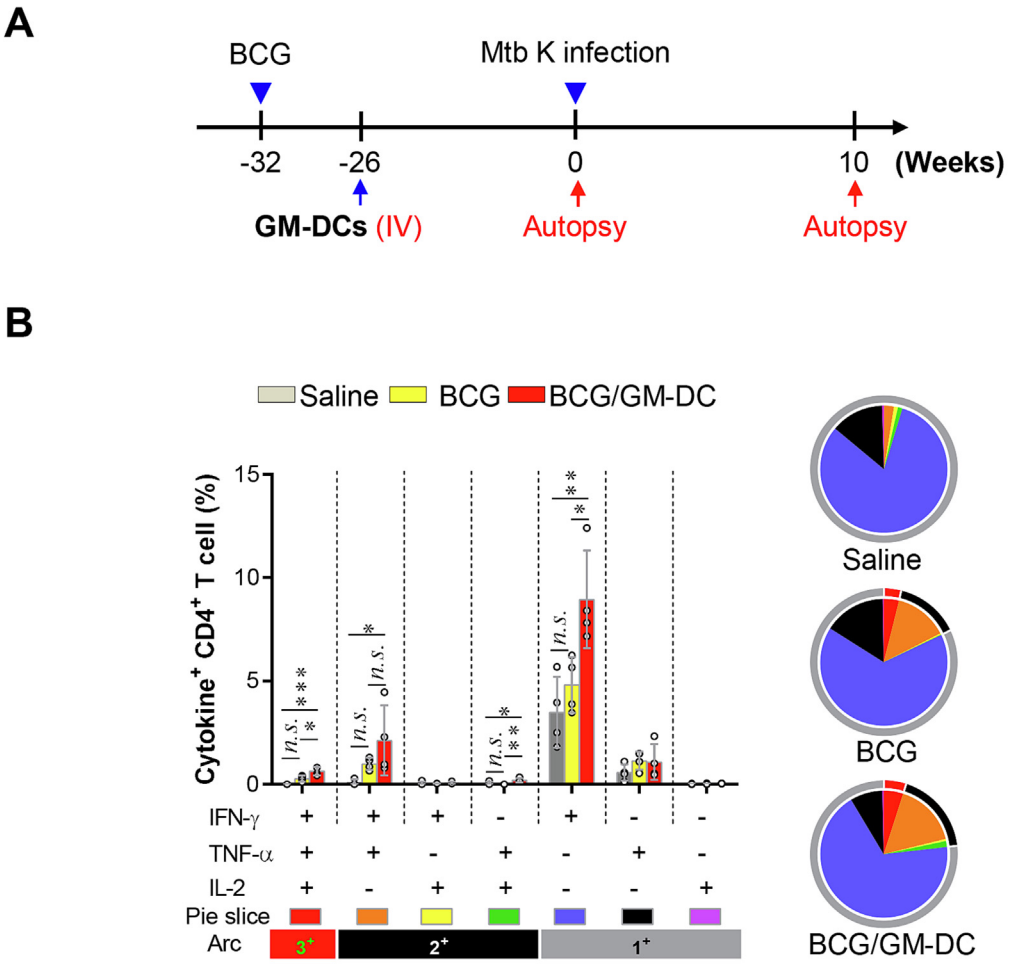

Fig. 5. Analysis of long-term protection in GM-DC-transferred mice after BCG vaccination against Mtb infection. (**A**) Six weeks after BCG vaccination, GM-DCs were administered to BCG-vaccinated mice. Twenty-six weeks later, the mice were infected with the Mtb K strain (120 CFUs/mouse). (**B**) Before Mtb K challenge, PPD-specific lung $CD4^+$ T cells producing the indicated cytokines were analyzed. The mean frequencies of cells co-producing IFN-γ, TNF-α, and/or IL-2 are represented in the pie charts. The arcs surrounding the pie charts denote the number of cytokines produced by the T cells. $n = 4$. (**C**) Ten weeks after Mtb K infection, the superior lobes of the right lung were analyzed using H&E staining, and bacterial growth in the lung and spleen (**D**) were depicted with bar graphs. $n = 4$. Data are mean ± SD. Statistical analysis was performed by one-way ANOVA with Tukey's multiple comparisons. *n.s.* = not significant, $^*p < 0.05$, $^{**}p < 0.01$, and $^{***}p < 0.001$.

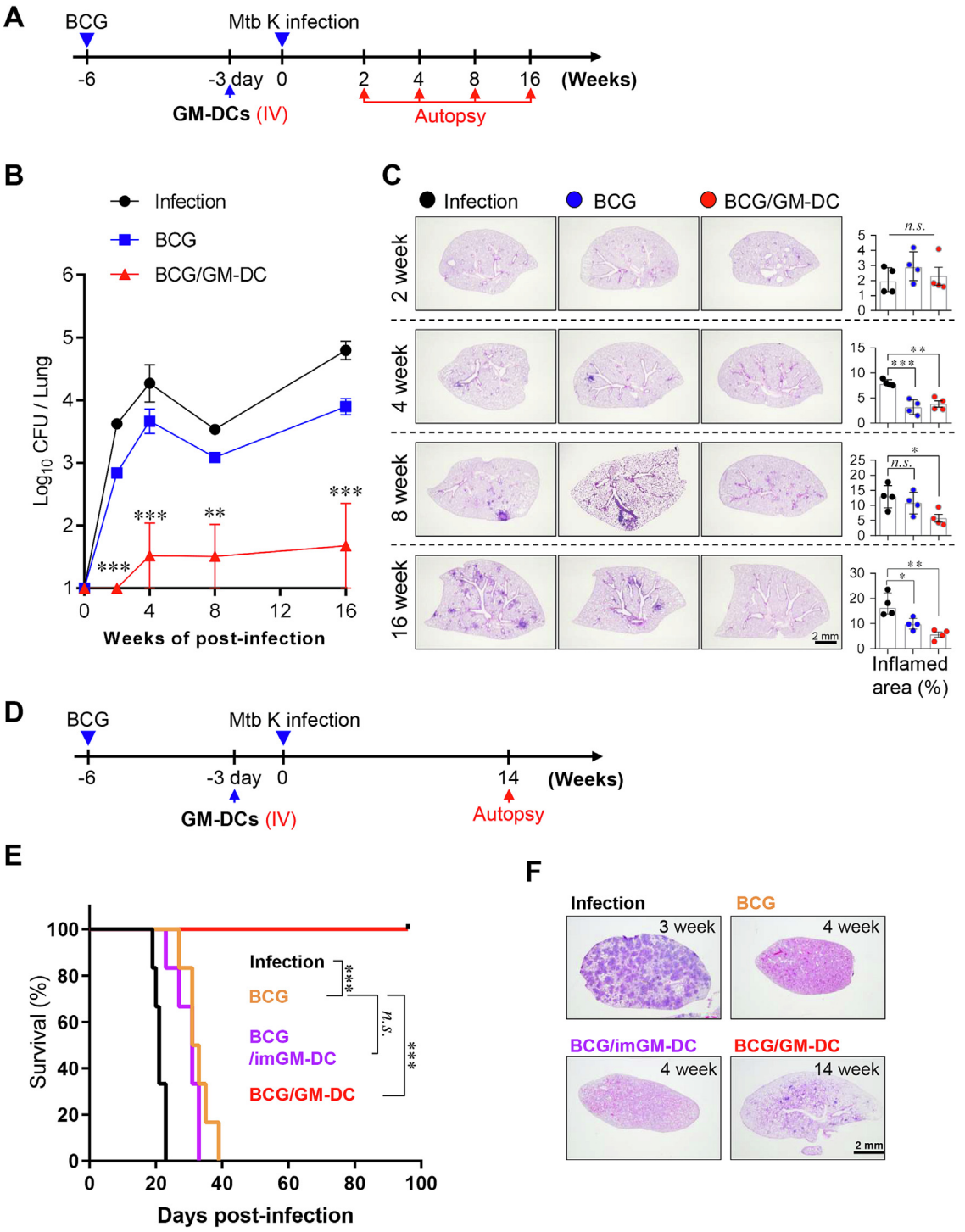

Fig. 6. Protective efficacy of GM-DC transfer in BCG-vaccinated mice against low dose and lethal dose Mtb infection. (**A**) BCG-immunized mice were transferred with GM-DC or saline. Three days after DC transfer, mice were challenged with a low dose (~10 CFUs/mouse) of Mtb K strain. (**B**) The lung bacterial growth was monitored at 2, 4, 8, and 16 weeks post-infection, and (**C**) lung histopathology at each sacrifice point was analyzed using H&E staining. $n = 4$. Data are mean ± SD. Statistical analysis was performed by one-way ANOVA with Tukey's multiple comparisons. *n.s.* = not significant, $^{**}p < 0.01$, $^{***}p < 0.001$. Asterisk without designation indicates comparison to BCG group. (**D**) For the lethal dose infection model, mice were challenged with a high dose (~1×10^5 CFUs/mouse) of Mtb K strain. (**E**) The survival of mice infected with Mtb K was tracked over a period of 14 weeks following infection. $n = 6$. Statistical analysis was performed by the Log-rank (Mantel-Cox) test. (**F**) Lung histopathology was evaluated at designated time points using H&E staining. The lung sections of the infection, BCG, and BCG/imGM-DC groups were stained after the mice succumbed to Mtb infection. imGM-DC, immature GM-DC.

(Fig. 7**C**). To evaluate the impact of combining GM-DC with antibiotics on lung pathology, histological analysis was performed on sections from the Abx, Abx + GM-DC, and Abx + imGM-DC groups at 12 weeks post-infection. Abx group showed pronounced pathological lesions in the lungs, while the Abx + GM-DC group exhibited diminished lung lesions. On the other hand, unlike GM-DC, the Abx + imGM-DC group had no beneficial effect on reducing pulmonary inflammation during antibiotic treatment (Fig. 7**D**). To evaluate the therapeutic effects of GM-DC administration combined with antibiotics, single-cell suspensions from lungs were

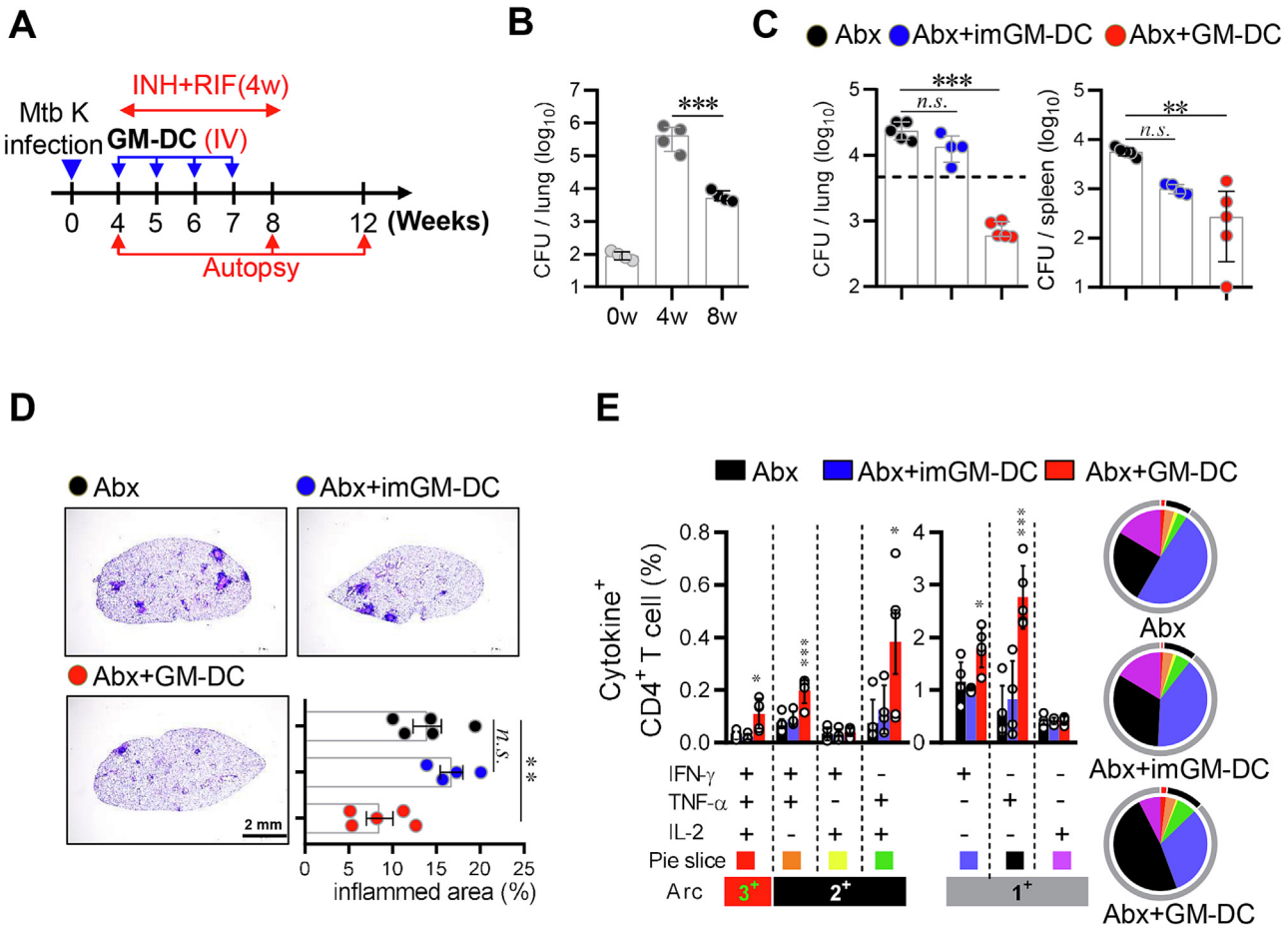

Fig. 7. Efficacy of GM-DC transfer as an adjunctive immunotherapy against TB during antibiotic treatment. (**A**) Mice were exposed to the Mtb K strain (~100 CFUs/mouse) and administered imGM-DC or GM-DC at 4, 5, 6, and 7 weeks post-infection. Antibiotics (Abx) treatment was carried out from 4 to 8 weeks post-infection. The lung bacterial growth was evaluated (**B**) at 4, 8, and (**C**) 12 weeks post-infection, and (**D**) the lung histopathology at 12 weeks post-infection were evaluated. n = 4–5. The dashed line represents the bacterial burden at 8 weeks post-infection after Abx treatment. (**E**) Twelve weeks post-infection, PPD-specific lung $CD4^+$ T cells producing the indicated cytokines were analyzed. n = 4–5. The mean frequencies of cells co-producing IFN-γ, TNF-α, and/or IL-2 are represented in the pie charts. The arcs surrounding the pie charts denote the number of cytokines produced by the T cells. Data are mean ± SD. Statistical analysis was performed by one-way ANOVA with Tukey's multiple comparisons. *n.s.* = not significant, $^*p < 0.05$, $^{**}p < 0.01$, and $^{***}p < 0.001$. Asterisk without designation indicates comparison to Abx group. Abx, isoniazid and rifampicin treatment.

stimulated with PPD. In the lungs of the Abx + GM-DC group, the frequency of $CD4^+$ T cells co-expressing IFN-γ, TNF-α, and IL-2, or IFN-γ and TNF-α, was higher compared to the Abx and Abx + imGM-DC groups (Fig. 7**E**). Conversely, the PPD-specific $CD8^+$ T cell response in the lung showed no significant differences among the groups (**Supplementary Fig. 15A**). Furthermore, the Abx + GM-DC group exhibited a modest increase in PPD-specific IgG1 levels compared to the Abx group, while PPD-specific IgG2c levels were significantly elevated in the Abx + GM-DC group (**Supplementary Fig. 15B**). In summary, these results indicate that GM-DC has the potential to enhance the efficacy of chemotherapy against Mtb infection by promoting a $CD4^+$ T cell-mediated Th1 immune response.

GM-DC administration during antibiotic treatment suppresses Mtb reactivation in drug-susceptible and drug-resistant TB models

To assess the effectiveness of GM-DC in combination with antibiotics for preventing Mtb reactivation, we utilized a modified version of the Cornell model, a widely recognized murine model for latent TB [45]. Mice infected with Mtb K were treated with INH and RIF starting at 4 weeks post-infection for a total duration of 8 weeks. GM-DC was administered once per week for 4 weeks, beginning 1 week before the completion of antibiotic treatment. After 23 and 35 weeks from infection, lung bacterial burden and pathology were analyzed (Fig. 8**A**). After 4 weeks from infection, lung bacterial burdens peaked at 5.59 $\log_{10}$ CFUs and progressively declined to nearly undetectable levels by 16 weeks post-infection. By 23 weeks post-infection, all mice in the Abx group experienced Mtb K reactivation, with lung bacterial counts escalating to 5.43 $\log_{10}$ CFUs by 35 weeks post-infection (Fig. 8**B**). Interestingly, Mtb K was detected in the lungs of one out of five mice (20 %, 1.30 $\log_{10}$ CFUs) and in the spleens of one out of five mice (20 %, 2.68 $\log_{10}$ CFUs) in the Abx + GM-DC group at 23 weeks post-infection (**Supplementary Fig. 16A**). Additionally, mild lung pathological lesions were detected in Abx group, whereas most pathological lesions were absent when combined with GM-DC treatment (Fig. 8**C**). To assess the long-term effects of GM-DC administration on Mtb reactivation, bacterial counts and histological analyses were performed on mouse tissues at 35 weeks post-infection, which corresponds to 23 weeks after completing an 8-week antibiotic treatment. As anticipated, the Abx + GM-DC group exhibited limited reactivation of Mtb K in lung tissue. In the Abx + GM-DC group, Mtb K was reactivated in the lungs of two out of six mice (33 %, 3.16 $\log_{10}$ CFUs) and in the spleens of three out of six mice (50 %, 2.31 $\log_{10}$ CFUs), respectively (**Supplemen-**

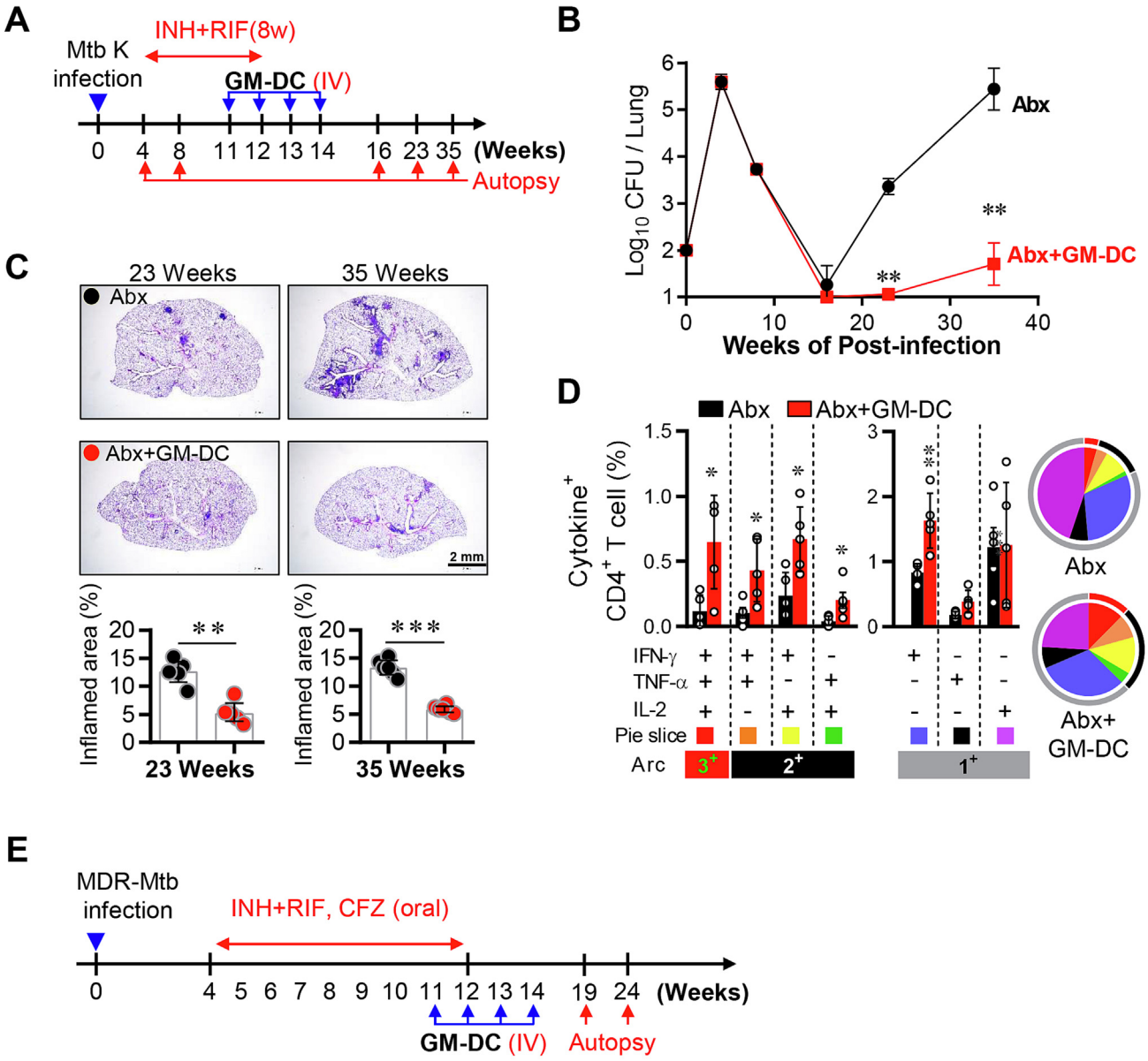
A
INH+RIF(8w)
Mtb K infection
GM-DC (IV)
0 4 8 11 12 13 14 16 23 35 (Weeks)
Autopsy
B
Log10 CFU / Lung
Abx
Abx+GM-DC
**
**
Weeks of Post-infection
C
23 Weeks
35 Weeks
Abx
Abx+GM-DC
2 mm
Inflamed area (%)
**
***
23 Weeks
35 Weeks
D
Abx
Abx+GM-DC
Cytokine+ CD4+ T cell (%)
IFN-γ
TNF-α
IL-2
Pie slice
Arc
3+
2+
1+
Abx
Abx+ GM-DC
E
MDR-Mtb infection
INH+RIF, CFZ (oral)
0 4 5 6 7 8 9 10 11 12 13 14 19 24 (Weeks)
GM-DC (IV)
Autopsy
F
Abx
Abx+GM-DC
2 mm
Inflamed area (%)
***
G
Saline
Abx (HR)
Abx (HRC)
Abx (HRC)+GM-DC
Log10 CFU / Lung
n.s.
***
Log10 CFU / Spleen
n.s.
***

tary Fig. 16A). Consistent with the bacterial growth results, lung pathological lesions were observed in the Abx group, whereas almost no lung lesions were observed in the Abx + GM-DC group at 23 and 35 weeks post-infection (Fig. 8**C**). Next, in order to characterize how GM-DC administration with antibiotics treatment affects immunological feature in Mtb reactivation, we evaluated the multifunctionality of PPD-specific lung T cells at 23 weeks post-infection. Compared to the Abx group, the Abx + GM-DC group showed increased frequency of PPD-specific lung $CD4^+$ T cells co-producing IFN-γ^+TNF-α^+IL-2^+, IFN-γ^+TNF-α^+, IFN-γ^+IL-2^+, and TNF-α^+IL-2^+ (Fig. 8**D**) but not in $CD8^+$ T cells (**Supplementary Fig. 16B**). In addition, the titers of PPD-specific IgG1 and IgG2c were higher in the Abx + GM-DC group than in Abx group (**Supplementary Fig. 16C**). These results suggest that during antibiotic therapy, the activation of $CD4^+$ T cell immunity through GM-DC transfer could enhance treatment effectiveness while suppressing Mtb reactivation.

Since MDR-TB requires more time and effort than other antibiotics regimens for treatment, a higher need for efficient treatment is urged. Thus, we explored the potential impact of GM-DC on MDR-TB reactivation using our previously established mouse model. The mice underwent an 8-week treatment regimen starting 4 weeks post-infection with either INH and RIF (HR) or INH, RIF, and CFZ (HRC) (Fig. 8**E**). Mice received weekly GM-DC administrations for 4 weeks, starting 1 week before the completion of antibiotic treatment. For the lung histopathological analysis, the lung sections were stained using H&E at 24 weeks post-infection. The Abx (HRC) group exhibited pathological lung lesions, whereas most mice in the Abx (HRC) + GM-DC group showed almost no inflamed areas (Fig. 8**F**). Bacterial presence in the lungs and spleens was undetectable in both the Abx (HRC) and Abx (HRC) + GM-DC groups at 19 weeks post-infection. By 24 weeks post-infection, lung bacterial CFUs reached 4.41 $\log_{10}$ in the Abx (HRC) group, while the Abx (HRC) + GM-DC group showed only 3.44 $\log_{10}$ CFUs, and the spleen bacterial growth exhibited a similar pattern to the lung (Fig. 8**G**). These results indicate that GM-DC administration during antibiotic therapy has a therapeutic potential against MDR-TB.

Discussion

For optimal TB control, both robust prevention and intensified therapeutic approaches must be prioritized [1,46]. The current BCG vaccine and conventional chemotherapy, though widely used, demonstrate inadequate efficacy. In this study, we propose advanced control strategies involving a BCG booster vaccine and adjunctive therapy with antibiotics, leveraging DCs. Our findings, demonstrated across multiple models, highlight the potential of DC-based interventions to enhance TB management on a comprehensive scale. Our results indicate that the GM-DC transfer, a BCG booster vaccine, induces T_{RM} in lung tissue, and promotes lung $CD4^+$ memory T cell response in the parenchymal area, accelerating the accumulation of protective Th1 cells from the initial phase of Mtb infection, and strengthens the efficacy of the BCG vaccine. Additionally, enhanced Ag-specific $CD4^+$ T cell responses by GM-DC transfer were also induced in an adjunctive therapy model, increasing the therapeutic efficacy of TB and mitigating reactivation. Furthermore, the ability of GM-DC transfer to suppress TB reactivation was validated in the MDR-TB model, demonstrating its therapeutic potential.

We confirmed that BCG/GM-DC vaccine has superior protective efficacy compared to BCG vaccine alone at 10 weeks after infection with the HN878 and K strains of the Beijing family (lineage 2) and the Erdman strain (lineage 4). Different Mtb strains exhibit a range of virulence levels, and the diversity in their phenotypic, genetic, and pathogenic potential could influence the efficacy of vaccines [16]. In particular, the Beijing strain (lineage 2), widespread in East Asia, is highly drug-resistant [47] and shows limited protection from the BCG vaccine, as observed in human and animal models [48,49]. While BCG offers initial protection, its efficacy declines substantially over time, particularly against highly pathogenic strains, emphasizing the importance of evaluating vaccines with clinical strains [16,49]. Furthermore, the observation that the BCG/GM-DC vaccine successfully maintained and even enhanced protective efficacy against these highly virulent clinical strains, particularly in the context of lineage 2 strains underscores its potential to overcome one of the major limitations of BCG alone.

$CD4^+$ T cells are central to host defense against active pulmonary TB, with protective responses closely associated with the localization of Mtb-specific $CD4^+$ T cells into the lung parenchymal region, where they interact with Mtb-infected macrophages [50]. However, Mtb strategically impairs the initiation of T cell responses during the early phase of infection [6], a phenomenon attributed to delayed Ag presentation by APCs, such as DCs [7,51]. The formation of memory T cells induced by vaccination enables the development of effective protective T cell responses against Mtb infection. Upon Ag exposure, these memory T cells can rapidly proliferate and differentiate into effector T cells. While T_{EM} provides short-term protection, T_{CM} are capable of conferring long-term immunity upon re-exposure to the pathogen. Lung T_{RM} is able to respond rapidly to infection because it resides directly in the lung tissue, the primary site of respiratory pathogen invasion. A recent study demonstrated that intravenously BCG-vaccinated *Macaca mulatta* exhibited prolonged recruitment of T cells and DCs to the airways up to the point of Mtb challenge, providing significantly greater protection compared to BCG-delivered intradermally or via mucosal routes [52]. Additionally, boosting immunization of H56:CAF01 and mucosal delivery of the BCG vaccine have been reported to significantly improve lung T_{RM} populations and potentiate early T cell responses against Mtb challenges [36]. In this study, we observed the formation of T_{CM}, T_{EM}, and T_{RM} in BCG-vaccinated mice was facilitated by the administration of

Fig. 8. Efficacy of adjunctive immunotherapy with GM-DC during antibiotic treatment in reactivation TB model with drug-sensitive Mtb and MDR-Mtb. (**A**) The mice were challenged with the Mtb K strain (~200 CFUs/mouse) and GM-DC was adoptively transferred once per week between 11 and 14 weeks post-infection. The Abx was administered from 4 weeks to 12 weeks of post-infection. (**B**) The bacterial burdens were measured at the indicated time points, and (**C**) lung histopathology was analyzed at 23 and 35 weeks of post-infection. $n = 5–6$. (**D**) At 23 weeks of post-infection PPD-specific lung $CD4^+$ T cells producing the indicated cytokines were analyzed. $n = 5$. The mean frequencies of cells co-producing IFN-γ, TNF-α, and/or IL-2 are represented in the pie charts. The arcs surrounding the pie charts denote the number of cytokines produced by the T cells. (**E**) The mice were aerosol challenged with the MDR-Mtb (A008, ~500 CFUs/mouse) and GM-DC was administered 4 times at 11, 12, 13, and 14 weeks post-infection. The Abx (HRC) were administered from 4 weeks to 12 weeks of post-infection. (**F**) The lung histopathology and (**G**) bacterial growth in the lung and spleen were analyzed at 24 weeks post-infection. $n = 4–7$. The dashed line represents the bacterial burden at 4 weeks post-infection before Abx (HRC) treatment. Data are mean ± SD. Statistical analysis was performed by unpaired Student's t-tests (between two groups) or one-way ANOVA with Tukey's post-test (between three or more groups). *n.s.* = not significant, $^*p < 0.05$, $^{**}p < 0.01$, and $^{***}p < 0.001$. Abx, isoniazid and rifampicin treatment; Abx (HRC), isoniazid, rifampicin, and clofazimine treatment.

GM-DCs. Additionally, we detected the localization of Ag-specific T cells in the lung parenchymal region and observed their accumulation in the mLN and spleen at 1 week post-infection. In addition to $CD4^+$ T cell responses, $CD8^+$ T cell responses were evaluated, and cytokine secretion by Ag-specific $CD8^+$ T cells was increased in the BCG/GM-DC group compared to the BCG-alone group. However, $CD4^+$ T cells exhibited a markedly stronger response, suggesting that the enhancement of BCG-induced vaccine efficacy by GM-DC transfer was primarily mediated through interactions with $CD4^+$ rather than $CD8^+$ T cells. This bias may stem from the pre-existing immunity shaped by BCG, which is poor at inducing $CD8^+$ T cell responses [35,53], and may be further amplified by GM-DC transfer.

Given the complexity of the lung immune microenvironment, it is also conceivable that other cell types beyond T cells contributed to the observed enhancement of vaccine efficacy. For example, alveolar macrophages (AMs) are particularly noteworthy, as they are the first cells to encounter inhaled Mtb and play a key role in regulating early immune responses [54]. Recent studies have shown that BCG vaccination can induce trained immunity in AMs, leading to improved antimicrobial activity upon secondary exposure [54]. Emerging evidence suggests that trained immunity is not limited to macrophages but also extends to other innate immune cells, such as natural killer cells [55], suggesting the critical role of innate immune cells in host protection. Although we did not directly investigate the involvement of innate immune cells in this study, GM-DC administration may indirectly influence the activation or function of innate immune cells. Considering the potential interplay between innate and adaptive immunity, this aspect may merit further investigation in future studies aimed at optimizing DC-based vaccine strategies.

In this study, BCG/GM-DC group vaccine showed superior protection against lethal dose challenge with Mtb, with no mortality, and provided more durable immunity against low-dose Mtb infection compared to the BCG group. The protective efficacy of this BCG/GM-DC strategy in the lethal dose challenge with Mtb model suggests its potential for use in high-risk TB environments [56]. Recent studies have reported that the BCG vaccine is capable of inducing sterilizing immunity in a subset of mice in an ultra-low dose Mtb infection model [44,57]. These findings suggest the possibility of achieving sterilizing immunity depending on the Mtb infection dose in mouse models. The successful induction of sterilizing immunity in low dose models is particularly relevant, as it reflects natural Mtb transmission conditions and supports the potential of the vaccine to prevent latent infection and progression to active TB. In this study, mice were infected with approximately 10 CFUs of Mtb. Following GM-DC boosting after BCG vaccination, bacteria were undetectable in the lungs of all but one mouse for up to 16 weeks post-infection. These findings indicate that DCs may serve as a potential target for inducing vaccine-mediated sterilizing immunity in a low dose infection mouse model. Consistent with our findings, a previous study demonstrated that intratracheal transfer of Ag85B-loaded DCs following BCG vaccination led to near-sterilizing immunity [25], supporting the potential of DC-based strategies to enhance vaccine efficacy against low dose Mtb infection.

In our study, repeated GM-DC transfers during antibiotic treatment induced a protective Th1 response, leading to reduced bacterial burdens in lung tissue, recovery from lung lesions, and a decreased relapse rate. *Mycobacterium indicus pranii*, a therapeutic vaccine currently in clinical trials, has demonstrated the capacity to elicit $CD4^+$ T cell responses during antibiotic treatment in a guinea pig model [58], supporting our results. In TB patients, antibiotic treatment promotes recovery by directly eliminating Mtb and suppressing inflammation. However, since most TB chemotherapeutic agents primarily target actively replicating bacilli, their effectiveness against non-replicating Mtb, which expresses stress- and dormancy-related genes, may be diminished [59]. Additionally, antibiotic treatment of active TB patients induces a decrease in proinflammatory cytokine release or Ag-specific Th1 responses, which play a key role in controlling bacilli [60]. This reduction could undermine the host's capacity to effectively manage Mtb infection. Furthermore, INH, one of the key drugs in TB chemotherapy, has been reported to diminish protective $CD4^+$ T cell responses [13]. Moreover, treatment for latent TB patients reduces multifunctional T cell responses in the blood [61]. These results suggest the importance of immunological intervention during TB chemotherapy, indicating that enhancement of effective T cell immunity could be pivotal in eradicating Mtb in conjunction with antibiotic treatment.

We adoptively transferred GM-DC in the late course of antibiotic treatment and elicited higher Ag-specific $CD4^+$ T cell responses despite lower Mtb bacterial counts than antibiotic treatment alone group in lung tissue at 23 weeks post-infection. These results suggest that GM-DC transfer concurrent with antibiotic treatment not only increases antibiotic treatment efficacy, but also that GM-DC delivery during late phase in antibiotic treatment may help overcome the loss of protective immune responses post-treatment and assist in controlling relapse. In our study, GM-DC transfer reduced recurrence relatively effectively when antibiotic-susceptible strains were treated, but the effect was less pronounced against MDR-TB strains. This disparity may be attributed to the specific antibiotics employed in the treatment [14]. A recent report suggests that CFZ, used in this study for MDR-Mtb, may diminish GM-DC efficacy by suppressing innate immune responses via NF-κB inhibition [14]. Another possible explanation could be the difference in the duration of antibiotic treatment or the timing of GM-DC administration, which may have influenced the overall therapeutic outcome. Thus, optimizing DC-based strategies, such as adjusting the timing of GM-DC transfer or controlling the number of GM-DCs administered, may improve treatment outcomes and relapse prevention in MDR-TB. Additionally, further combination studies with other MDR drugs, such as bedaquiline, pretomanid, and linezolid, are needed to refine treatment approaches [62]. Furthermore, advancing antibiotic treatment through immunological interventions will require further research on how individual antibiotics influence host immunity during TB treatment, which will be essential for developing more effective therapeutic strategies.

There are several limitations to the present study. First, our *in vivo* models were conducted using the C57BL/6 mouse strain. Alternative models such as the Kramnik mouse, which is more susceptible to Mtb infection and develops necrotic granulomas resembling human TB pathology [63], may allow for a more comprehensive evaluation of DC-based TB control strategies. Furthermore, the Collaborative Cross mouse model [64] which captures the genetic and immunological diversity of TB, as well as more physiologically relevant models such as non-human primates, could provide additional insights into the translational potential of this approach. Expanding future evaluations to these models would help validate the robustness and generalizability of DC-based TB control strategies across diverse host contexts. Second, there are difficulties in practical application of the TB control strategy presented in this study. The practical application of DC-based TB control strategies faces challenge, as loading and re-administering Mtb-Ag using DCs differentiated from autologous cells increases procedural complexity, time, and financial costs. Recently, it was reported that a TLR-2 ligand-coated nanoparticle vaccine loaded with TB epitopes targeting DCs can induce anti-TB immunity [65]. Furthermore, research has shown that the limitations of DC cancer therapy can be addressed using artificial nanodendritic cells [66]. Artificial nanodendritic cells were created

by integrating the membrane of DC onto gold nanoparticles, effectively stimulating a tumor-specific T cell immune response. Nanoparticle-based DC-targeting strategies or artificial nanodendritic cells may serve as practical alternatives to *ex vivo*-generated DC approaches. Unlike cell-based platforms that require the isolation and differentiation of autologous DCs from peripheral blood, these synthetic or *in vivo*-targeting systems eliminate the need for individualized cell processing, thereby overcoming temporal, logistical, and spatial constraints. Although such strategies may not fully replicate the functional and phenotypic characteristics of naturally differentiated DCs, demonstrated immunogenicity at a sufficient level has the potential to significantly lower the barriers to clinical translation and to enable broader application across patient populations. Third, since CFA is a mixture containing Ags that are unnecessary or may suppress protective immunity, a better strategy could involve Ag down-selection and integration according to stage-specific purposes, using only the key vaccine Ags or those specifically capable of preventing reactivation after treatment. However, clearly defined protective Ags for TB have yet to be identified. Notably, vaccine candidates such as H56: IC31 and MVA85A, despite demonstrating efficacy in preclinical animal models, failed to achieve their intended outcomes in clinical trials [67,68]. The identification of truly protective Ags would warrant the practical application of such targeted strategies. In this study, we employed CFA in this study to broadly boost immunity against the diverse antigenic repertoire present in BCG.

Fourth, in our study, we did not include a BCG-prime/BCG-booster vaccination (BCG revaccination) group. To date, studies investigating BCG revaccination have yielded conflicting results [69,70], with outcomes varying depending on study design and population. Nonetheless, BCG revaccination remains an important strategy, as enhancing the protective efficacy of BCG could provide a valuable tool for global TB control. BCG could suppress several stages of the innate immune response, which may limit its capacity to induce robust Ag presentation and long-term immune memory. Therefore, comparative analysis between BCG alone, BCG revaccination, and BCG with GM-DC administration may help to understand the role of DC-based activation and develop optimized BCG-based strategies. Fifth, since the BCG vaccine is typically administered in early infancy, the experiments in this study only considered scenarios where BCG was given first. Therefore, the study does not fully address the effects of administering DCs before BCG vaccination. Additionally, to evaluate the age-dependent efficacy of the BCG/GM-DC vaccine strategy, GM-DCs were transferred at different time points following BCG vaccination performed at 6–7 weeks of age, specifically at 6 weeks (13 weeks old), 10 weeks (17 weeks old), and 30 weeks (37 weeks old) post-vaccination. Previous studies showing that the efficacy of BCG in an aged mouse model is comparable to that in a young mouse model [71,72] suggest the possibility of GM-DC transfer after BCG vaccination in aged mice, but the efficacy in mice of different ages requires further study. Lastly, reference biomarkers are needed for a more effective DC-based TB control strategy. In animal models, infected lung tissues can be directly analyzed to assess immune responses; however, such approaches are not feasible in humans. Therefore, evaluating immune signatures in peripheral blood, such as gene expression or cytokine profiles, represents a more practical and clinically applicable approach. Although this study was limited to analyses of infected tissues such as the lung and spleen, identifying blood-based biomarkers that can predict the efficacy of BCG/GM-DC immunotherapy would greatly facilitate clinical translation. In our study, GM-DCs were transferred either concurrently with antibiotics to improve treatment efficacy or shortly before antibiotic completion to reduce recurrence. However, reference biomarkers are needed for more effective treatment strategies to determine the optimal timing for initiating DC-based therapies, their duration, and when to discontinue them. Additionally, as GM-DC administration during antibiotic treatment may trigger excessive inflammatory responses, biomarkers are warranted to monitor treatment efficacy and disease severity during therapy.

These blood-based biomarkers may provide guidelines for immunological intervention during antibiotic treatment.

Conclusion

In conclusion, our findings present effective DC-based strategies for combating Mtb infection. The transfer of GM-DCs enhanced BCG efficacy, as demonstrated across several clinical strains and relevant models. This approach also promoted the localization of Ag-specific multifunctional lung $CD4^+$ T cells in parenchymal region at the initial infection stage. Additionally, GM-DC transfer during antibiotic treatment enhanced treatment outcomes, suppressed reactivation, and showed notable efficacy against both drug-sensitive Mtb and MDR-Mtb infections. These results emphasize the pivotal role of DCs in TB prevention and treatment, offering valuable insights into addressing the limitations of current BCG vaccines and antibiotic therapies. This approach offers potential for addressing the broad spectrum of TB, diminishing BCG efficacy, TB reactivation, and the substantial challenges of MDR-TB management. Additional studies are needed to comprehensively evaluate the long-term efficacy and safety of DC-based strategies across diverse patient populations and clinical settings.

Declaration of competing interest

The authors declare that they have no known competing financial interests or personal relationships that could have appeared to influence the work reported in this paper.

Acknowledgments

This work was supported by the National Research Foundation of Korea (NRF) grant funded by the Korea government (MSIT) (RS-2023-00208115), and by a grant of the Korea Health Technology R&D Project through the Korea Health Industry Development Institute (KHIDI), funded by the Ministry of Health & Welfare, Republic of Korea (RS-2025-02173063). The funders were not involved in the study design, data collection, analysis, decision to publish, or manuscript preparation.

Author contributions

Conceptualization: SJS.
Methodology: SJS, JSK, WSK, HK, KWK, MP, SC, JK.
Investigation: WSK, JSK, HK.
Visualization: WSK, JSK, HK, SC, JK.
Supervision: SJS.
Writing—original draft: SJS, JSK, HK.
Writing—review & editing: WSK, JSK, HK, SJH, SJS.

Availability of data and materials.

All data necessary to support the conclusions of this paper are included within the paper and/or the Supplementary Materials. Raw sequencing data are available at the NCBI Sequence Read Archive under BioProject accession number PRJNA1188216.

Appendix A. Supplementary data

Supplementary data to this article can be found online at https://doi.org/10.1016/j.jare.2025.07.056.

References

[1] Organization WH. Global tuberculosis report 2024. Geneva: World Health Organization; 2024.
[2] Colditz GA, Berkey CS, Mosteller F, Brewer TF, Wilson ME, Burdick E, et al. The efficacy of bacillus Calmette-Guérin vaccination of newborns and infants in the prevention of tuberculosis: meta-analyses of the published literature. Pediatrics 1995;96(1 Pt 1):29–35.
[3] Dheda K, Gumbo T, Maartens G, Dooley KE, McNerney R, Murray M, et al. The epidemiology, pathogenesis, transmission, diagnosis, and management of multidrug-resistant, extensively drug-resistant, and incurable tuberculosis. Lancet Respir Med 2017. doi: https://doi.org/10.1016/s2213-2600(17)30079-6.
[4] . Eur Respir J 2022;59(3).
[5] Chiok KR, Dhar N, Banerjee A. *Mycobacterium tuberculosis* and SARS-CoV-2 co-infections: The knowns and unknowns. iScience 2023;26(5):106629.
[6] Liu X, Yang M, Xu P, Du M, Li S, Shi J, et al. Kynurenine-AhR reduces T-cell infiltration and induces a delayed T-cell immune response by suppressing the STAT1-CXCL9/CXCL10 axis in tuberculosis. Cell Mol Immunol 2024. doi: https://doi.org/10.1038/s41423-024-01230-1.
[7] Srivastava S, Grace PS, Ernst JD. Antigen Export Reduces Antigen Presentation and Limits T Cell Control of *M. tuberculosis*. Cell Host Microbe 2016;19(1):44–54.
[8] Koh VH, Ng SL, Ang ML, Lin W, Ruedl C, Alonso S. Role and contribution of pulmonary CD103(+) dendritic cells in the adaptive immune response to *Mycobacterium tuberculosis*. Tuberculosis (Edinb) 2017;102:34–46.
[9] Lai R, Jeyanathan M, Afkhami S, Zganiacz A, Hammill JA, Yao Y, et al. CD11b(+) Dendritic Cell-Mediated Anti-*Mycobacterium tuberculosis* Th1 Activation is Counterregulated by CD103(+) Dendritic Cells via IL-10. J Immunol 2018;200(5):1746–60.
[10] Gupta A, Ahmad FJ, Ahmad F, Gupta UD, Natarajan M, Katoch VM, et al. Protective efficacy of *Mycobacterium indicus pranii* against tuberculosis and underlying local lung immune responses in guinea pig model. Vaccine 2012;30(43):6198–209.
[11] Coler RN, Bertholet S, Pine SO, Orr MT, Reese V, Windish HP, et al. Therapeutic immunization against *Mycobacterium tuberculosis* is an effective adjunct to antibiotic treatment. J Infect Dis 2013;207(8):1242–52.
[12] Condos R, Rom WN, Schluger NW. Treatment of multidrug-resistant pulmonary tuberculosis with interferon-gamma via aerosol. Lancet 1997;349(9064):1513–5.
[13] Tousif S, Singh DK, Ahmad S, Moodley P, Bhattacharyya M, Van Kaer L, et al. Isoniazid induces apoptosis of activated $CD4^+$ T cells: implications for post-therapy tuberculosis reactivation and reinfection. J Biol Chem 2014;289(44):30190–5.
[14] Li X, Luo X, Wang B, Fu L, Chen X, Lu Y. Clofazimine inhibits innate immunity against *Mycobacterium tuberculosis* by NF-κB. mSphere 2024;9(8):e0025424.
[15] Esmail H, Macpherson L, Coussens AK, Houben R. Mind the gap - managing tuberculosis across the disease spectrum. EBioMedicine 2022;78:103928.
[16] Jeon BY, Derrick SC, Lim J, Kolibab K, Dheenadhayalan V, Yang AL, et al. *Mycobacterium bovis* BCG immunization induces protective immunity against nine different *Mycobacterium tuberculosis* strains in mice. Infect Immun 2008;76(11):5173–80.
[17] Burman WJ, Bliven EE, Cowan L, Bozeman L, Nahid P, Diem L, et al. Relapse associated with active disease caused by Beijing strain of *Mycobacterium tuberculosis*. Emerg Infect Dis 2009;15(7):1061–7.
[18] Li QJ, Jiao WW, Yin QQ, Li YJ, Li JQ, Xu F, et al. Positive epistasis of major low-cost drug resistance mutations *rpoB*531-TTG and *katG*315-ACC depends on the phylogenetic background of *Mycobacterium tuberculosis* strains. Int J Antimicrob Agents 2017;49(6):757–62.
[19] Harding JS, Schreiber HA, Sandor M. Granuloma transplantation: an approach to study mycobacterium-host interactions. Front Microbiol 2011;2:245.
[20] Harding JS, Rayasam A, Schreiber HA, Fabry Z, Sandor M. Mycobacterium-Infected Dendritic Cells Disseminate Granulomatous Inflammation. Sci Rep 2015;5:15248.
[21] Panda S, Morgan J, Cheng C, Saito M, Gilman RH, Ciobanu N, et al. Identification of differentially recognized T cell epitopes in the spectrum of tuberculosis infection. Nat Commun 2024;15(1):765.
[22] Velasquez LN, Stüve P, Gentilini MV, Swallow M, Bartel J, Lycke NY, et al. Targeting *Mycobacterium tuberculosis* Antigens to Dendritic Cells via the DC-specific-ICAM3-Grabbing-Nonintegrin Receptor Induces strong T-Helper 1 Immune responses. Front Immunol 2018;9:471.
[23] Griffiths KL, Ahmed M, Das S, Gopal R, Horne W, Connell TD, et al. Targeting dendritic cells to accelerate T-cell activation overcomes a bottleneck in tuberculosis vaccine efficacy. Nat Commun 2016;7:13894.
[24] Larsen SE, Baldwin SL, Orr MT, Reese VA, Pecor T, Granger B, et al. Enhanced Anti-*Mycobacterium tuberculosis* Immunity over Time with combined Drug and Immunotherapy Treatment. Vaccines (Basel) 2018;6(2).
[25] Shin AR, Kim HJ, Cho SN, Collins MT, Manning EJ, Naser SA, et al. Identification of seroreactive proteins in the culture filtrate antigen of *Mycobacterium avium* ssp. paratuberculosis human isolates to sera from Crohn's disease patients. FEMS Immunol Med Microbiol 2010;58(1):128–37.
[26] Han SJ, Song T, Cho YJ, Kim JS, Choi SY, Bang HE, et al. Complete genome sequence of *Mycobacterium tuberculosis* K from a Korean high school outbreak, belonging to the Beijing family. Stand Genomic Sci 2015;10:78.
[27] Kim JS, Kang MJ, Kim WS, Han SJ, Kim HM, Kim HW, et al. Essential engagement of Toll-like receptor 2 in initiation of early protective Th1 response against rough variants of *Mycobacterium abscessus*. Infect Immun 2015;83(4):1556–67.
[28] Cha SB, Kim WS, Kim JS, Kim H, Kwon KW, Han SJ, et al. Pulmonary immunity and durable protection induced by the ID93/GLA-SE vaccine candidate against the hyper-virulent Korean Beijing *Mycobacterium tuberculosis* strain K. Vaccine 2016;34(19):2179–87.
[29] Mokrousov I, Vinogradova T, Dogonadze M, Zabolotnykh N, Vyazovaya A, Vitovskaya M, et al. A multifaceted interplay between virulence, drug resistance, and the phylogeographic landscape of *Mycobacterium tuberculosis*. Microbiol Spectr 2023;11(5):e0139223.
[30] Jeon BY, Kwak J, Hahn MY, Eum SY, Yang J, Kim SC, et al. In vivo characteristics of Korean Beijing *Mycobacterium tuberculosis* strain K1 in an aerosol challenge model and in the Cornell latent tuberculosis model. J Med Microbiol 2012;61(Pt 10):1373–9.
[31] Jeon BY, Kim SC, Eum SY, Cho SN. The immunity and protective effects of antigen 85A and heat-shock protein X against progressive tuberculosis. Microbes Infect 2011;13(3):284–90.
[32] Kim H, Shin SJ. Pathological and protective roles of dendritic cells in *Mycobacterium tuberculosis* infection: Interaction between host immune responses and pathogen evasion. Front Cell Infect Microbiol 2022;12:891878.
[33] Brasel K, De Smedt T, Smith JL, Maliszewski CR. Generation of murine dendritic cells from flt3-ligand-supplemented bone marrow cultures. Blood 2000;96(9):3029–39.
[34] Woodworth JS, Clemmensen HS, Battey H, Dijkman K, Lindenstrøm T, Laureano RS, et al. A *Mycobacterium tuberculosis*-specific subunit vaccine that provides synergistic immunity upon co-administration with bacillus Calmette-Guérin. Nat Commun 2021;12(1):6658.
[35] Gröschel MI, Sayes F, Shin SJ, Frigui W, Pawlik A, Orgeur M, et al. Recombinant BCG Expressing ESX-1 of *Mycobacterium marinum* Combines Low Virulence with Cytosolic Immune Signaling and improved TB Protection. Cell Rep 2017;18(11):2752–65.
[36] Woodworth JS, Christensen D, Cassidy JP, Agger EM, Mortensen R, Andersen P. Mucosal boosting of H56:CAF01 immunization promotes lung-localized T cells and an accelerated pulmonary response to *Mycobacterium tuberculosis* infection without enhancing vaccine protection. Mucosal Immunol 2019;12(3):816–26.
[37] Sakai S, Kauffman KD, Schenkel JM, McBerry CC, Mayer-Barber KD, Masopust D, et al. Cutting edge: control of *Mycobacterium tuberculosis* infection by a subset of lung parenchyma-homing CD4 T cells. J Immunol 2014;192(7):2965–9.
[38] Szabo PA, Miron M, Farber DL. Location, location, location: Tissue resident memory T cells in mice and humans. Sci Immunol 2019;4(34).
[39] Shanmugasundaram U, Bucsan AN, Ganatra SR, Ibegbu C, Quezada M, Blair RV, et al. Pulmonary *Mycobacterium tuberculosis* control associates with CXCR3- and CCR6-expressing antigen-specific Th1 and Th17 cell recruitment. JCI Insight 2020;5(14).
[40] Gopal R, Lin Y, Obermajer N, Slight S, Nuthalapati N, Ahmed M, et al. IL-23-dependent IL-17 drives Th1-cell responses following *Mycobacterium bovis* BCG vaccination. Eur J Immunol 2012;42(2):364–73.
[41] Lindenstrøm T, Knudsen NP, Agger EM, Andersen P. Control of chronic *mycobacterium tuberculosis* infection by CD4 KLRG1- IL-2-secreting central memory cells. J Immunol 2013;190(12):6311–9.
[42] McKinstry KK, Strutt TM, Bautista B, Zhang W, Kuang Y, Cooper AM, et al. Effector CD4 T-cell transition to memory requires late cognate interactions that induce autocrine IL-2. Nat Commun 2014;5:5377.
[43] Chang E, Cavallo K, Behar SM. CD4 T cell dysfunction is associated with bacterial recrudescence during chronic tuberculosis. Nat Commun 2025;16(1):2636.
[44] Plumlee CR, Duffy FJ, Gern BH, Delahaye JL, Cohen SB, Stoltzfus CR, et al. Ultra-low Dose Aerosol Infection of mice with *Mycobacterium tuberculosis* more closely Models Human Tuberculosis. Cell Host Microbe 2021;29(1):68–82.e5.
[45] Scanga CA, Mohan VP, Joseph H, Yu K, Chan J, Flynn JL. Reactivation of latent tuberculosis: variations on the Cornell murine model. Infect Immun 1999;67(9):4531–8.
[46] An Y, Ni R, Zhuang L, Yang L, Ye Z, Li L, et al. Tuberculosis vaccines and therapeutic drug: challenges and future directions. Mol Biomed 2025;6(1):4.
[47] Parwati I, van Crevel R, van Soolingen D. Possible underlying mechanisms for successful emergence of the *Mycobacterium tuberculosis* Beijing genotype strains. Lancet Infect Dis 2010;10(2):103–11.
[48] Verrall AJ, Chaidir L, Ruesen C, Apriani L, Koesoemadinata RC, van Ingen J, et al. Lower bacillus Calmette-Guérin Protection against *Mycobacterium tuberculosis* Infection after Exposure to Beijing Strains. Am J Respir Crit Care Med 2020;201(9):1152–5.
[49] Ordway DJ, Shang S, Henao-Tamayo M, Obregon-Henao A, Nold L, Caraway M, et al. *Mycobacterium bovis* BCG-mediated protection against W-Beijing strains of *Mycobacterium tuberculosis* is diminished concomitant with the emergence of regulatory T cells. Clin Vaccine Immunol 2011;18(9):1527–35.
[50] Santiago-Carvalho I, Almeida-Santos G, Macedo BG, Barbosa-Bomfim CC, Almeida FM, Pinheiro Cione MV, et al. T cell-specific P2RX7 favors lung parenchymal CD4(+) T cell accumulation in response to severe lung infections. Cell Rep 2023;42(11):113448.
[51] Urdahl KB. Understanding and overcoming the barriers to T cell-mediated immunity against tuberculosis. Semin Immunol 2014;26(6):578–87.

[52] Darrah PA, Zeppa JJ, Maiello P, Hackney JA, Wadsworth 2nd MH, Hughes TK, et al. Prevention of tuberculosis in macaques after intravenous BCG immunization. Nature 2020;577(7788):95–102.
[53] Ryan AA, Nambiar JK, Wozniak TM, Roediger B, Shklovskaya E, Britton WJ, et al. Antigen load governs the differential priming of CD8 T cells in response to the bacille Calmette Guerin vaccine or *Mycobacterium tuberculosis* infection. J Immunol 2009;182(11):7172–7.
[54] Mai D, Jahn A, Murray T, Morikubo M, Lim PN, Cervantes MM, et al. Exposure to Mycobacterium remodels alveolar macrophages and the early innate response to *Mycobacterium tuberculosis* infection. PLoS Pathog 2024;20(1):e1011871.
[55] Nieto Ramirez LM, Mehaffy C, Dobos KM. Systematic review of innate immune responses against *Mycobacterium tuberculosis* complex infection in animal models. Front Immunol 2024;15:1467016.
[56] van Rie A, McCarthy K, Scott L, Dow A, Venter WD, Stevens WS. Prevalence, risk factors and risk perception of tuberculosis infection among medical students and healthcare workers in Johannesburg. South Africa S Afr Med J 2013;103(11):853–7.
[57] Plumlee CR, Barrett HW, Shao DE, Lien KA, Cross LM, Cohen SB, et al. Assessing vaccine-mediated protection in an ultra-low dose *Mycobacterium tuberculosis* murine model. bioRxiv 2023. doi: https://doi.org/10.1101/2023.03.22.533820.
[58] Gupta A, Ahmad FJ, Ahmad F, Gupta UD, Natarajan M, Katoch V, et al. Efficacy of *Mycobacterium indicus pranii* immunotherapy as an adjunct to chemotherapy for tuberculosis and underlying immune responses in the lung. PLoS One 2012;7(7):e39215.
[59] Mehra S, Foreman TW, Didier PJ, Ahsan MH, Hudock TA, Kissee R, et al. The DosR Regulon Modulates Adaptive Immunity and is Essential for *Mycobacterium tuberculosis* Persistence. Am J Respir Crit Care Med 2015;191(10):1185–96.
[60] Mattos AM, Almeida Cde S, Franken KL, Alves CC, Abramo C, de Souza MA, et al. Increased IgG1, IFN-gamma, TNF-alpha and IL-6 responses to *Mycobacterium tuberculosis* antigens in patients with tuberculosis are lower after chemotherapy. Int Immunol 2010;22(9):775–82.
[61] Sauzullo I, Mengoni F, Mascia C, Rossi R, Lichtner M, Vullo V, et al. Treatment of latent tuberculosis infection induces changes in multifunctional *Mycobacterium tuberculosis*-specific $CD4^+$ T cells. Med Microbiol Immunol 2016;205(1):37–45.
[62] Karnan A, Jadhav U, Ghewade B, Ledwani A, Shivashankar P. A Comprehensive Review on Long vs. Short Regimens in Multidrug-Resistant Tuberculosis (MDR-TB) under Programmatic Management of Drug-Resistant Tuberculosis (PMDT). Cureus 2024;16(1):e52706.
[63] Kramnik I, Beamer G. Mouse models of human TB pathology: roles in the analysis of necrosis and the development of host-directed therapies. Semin Immunopathol 2016;38(2):221–37.
[64] Smith CM, Baker RE, Proulx MK, Mishra BB, Long JE, Park SW, et al. Host-pathogen genetic interactions underlie tuberculosis susceptibility in genetically diverse mice. Elife 2022;11.
[65] Kumar Das D, Zafar MA, Nanda S, Singh S, Lamba T, Bashir H, et al. Targeting dendritic cells with TLR-2 ligand-coated nanoparticles loaded with *Mycobacterium tuberculosis* epitope induce antituberculosis immunity. J Biol Chem 2022;298(12):102596.
[66] Choi D, Kang TG, Kim T, Moon C-W, Choi M, Kim D-H, et al. Immortalized nanodendritic cells decorated with immune-checkpoint inhibitors for personalized cancer immunotherapy. Nano Today 2024;56:102237.
[67] Tameris MD, Hatherill M, Landry BS, Scriba TJ, Snowden MA, Lockhart S, et al. Safety and efficacy of MVA85A, a new tuberculosis vaccine, in infants previously vaccinated with BCG: a randomised, placebo-controlled phase 2b trial. Lancet 2013;381(9871):1021–8.
[68] Borges ÁH, Russell M, Tait D, Scriba TJ, Nemes E, Skallerup P, et al. Immunogenicity, safety, and efficacy of the vaccine H56:IC31 in reducing the rate of tuberculosis disease recurrence in HIV-negative adults successfully treated for drug-susceptible pulmonary tuberculosis: a double-blind, randomised, placebo-controlled, phase 2b trial. Lancet Infect Dis 2025;25(7):751–63.
[69] Leung CC, Tam CM, Chan SL, Chan-Yeung M, Chan CK, Chang KC. Efficacy of the BCG revaccination programme in a cohort given BCG vaccination at birth in Hong Kong. Int J Tuberc Lung Dis 2001;5(8):717–23.
[70] Nemes E, Geldenhuys H, Rozot V, Rutkowski KT, Ratangee F, Bilek N, et al. Prevention of *M. tuberculosis* Infection with H4:IC31 Vaccine or BCG Revaccination. N Engl J Med 2018;379(2):138–49.
[71] Ito T, Takii T, Maruyama M, Hayashi D, Wako T, Asai A, et al. Effectiveness of BCG vaccination to aged mice. Immun Ageing 2010;7:12.
[72] Ozeki Y, Hirayama Y, Takii T, Yamamoto S, Kobayashi K, Matsumoto S. Loss of anti-mycobacterial efficacy in mice over time following vaccination with *Mycobacterium bovis* bacillus Calmette-Guérin. Vaccine 2011;29(40):6881–7.